Microdomain Scale Organization and Scattering Patterns of Associating Polymer Melts

Kathleen A. Kolbet and Kenneth S. Schweizer*

Departments of Chemistry and Materials Science & Engineering, and Materials Research Laboratory, University of Illinois, 1304 West Green Street, Urbana, Illinois 61801

Received August 3, 1999; Revised Manuscript Received December 7, 1999

ABSTRACT: A microscopic theory of the structure of compressible associating AB regular heteropolymer fluids is proposed based on polymer integral equation methods. The theory is employed to systematically explore, as a function of temperature, the influence of sticky group attractive energy, concentration, degree of blockiness, and global architecture (telechelic, surfactant, multiblock) on self-assembly and microdomain formation as encoded in small-angle partial scattering structure factors. Characteristic apparent spinodal and order−disorder temperatures are estimated, and strong composition fluctuation effects are always present. The evolution of collective properties derived from scattering profiles such as microdomain period, intermultiplet coherence length, degree of Porodlike scattering, and modification of wide-angle intensity, with polymer structure and thermodynamic state are established. At fixed bare (chemical) driving force, end-functionalized architectures are found to form more ordered microphase-separated fluids than the multiblock analogues. Increasing sequence length also enhances self-assembly even at fixed global sticky group composition. Significant differences between telechelics composed of unimer sticky groups vs mini-triblocks are found, with the former displaying many self-assembly features not in accord with classic block copolymer behavior. Semiquantitative comparisons with small-angle X-ray scattering experiments suggest the theory provides a realistic description of self-assembly in ionomer melts, and failure of incompressible random phase approximation approaches for many properties is documented. Predictions for the majority (nonpolar) monomer density fluctuations, and cross-correlations, are obtained. Subtle, but systematic structural changes are induced by the minority group self-assembly process which may be amenable to direct measurement using small-angle neutron scattering and are possibly of mechanical property relevance.

I. Introduction

Polymeric fluids composed of AB heteropolymers where the B monomers experience strong attractive interactions are experimentally realized in diblock and triblock copolymers dissolved in selective solvents, ionomer solutions and melts, and aqueous water solutions of hydrophobic−hydrophilic copolymers.[1] These "associating polymers" can spontaneously self-assemble into various microdomain structures with different equilibrium and mechanical properties.[2−14] Ionomers are copolymers generally consisting of a nonpolar backbone and less than ≅10% of neutralizable acid groups.[1] In their pure acid form the minority "sticky B groups" interact via hydrogen bonds of moderate strength ϵ_{BB}; when neutralized by the metal cation of a salt, strong dipolar attractions ($\epsilon_{BB} \gg$ thermal energy, k_BT) can be realized. These materials are of considerable technological interest as thermoplastics, membranes, and networks.[1] Synthetic control can be exerted over the fraction and interaction strength of the strongly attractive groups, arrangement into blocky sequences, regular vs random arrangement of sticky groups, and the global architecture (e.g., surfactant, telechelic, multiblock). A drawing of some of the possibilities studied in this work is shown in Figure 1. Although our work is relevant to a variety of dense associating polymer fluids, our primary interest in this paper is ionomer melts, and we discuss the theory in this context. In contrast to diblock copolymers,[15] long-range order is not attained in ionomer melts. Rather, relatively small aggregates of the sticky groups on different chains (often called "multiplets" and estimated to consist of eight or less ion pairs or dipoles)[1,16,17] are formed via physical clustering. The corresponding microdomains are strongly spatially correlated but in a *globally isotropic* liquidlike manner.[1,18] Such collective structure has been probed primarily by

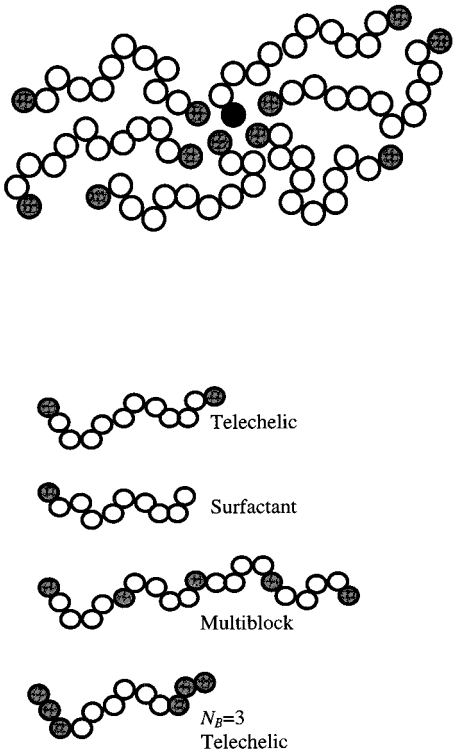

Figure 1. Schematic illustration of cluster formation in telechelic ionomer melts and the different types of associating polymer models considered in this work.

10.1021/ma9912913 CCC: $19.00
Published on Web 01/27/2000

X-ray scattering since the multiplets are believed to be only of the order of 10 Å in radius and thus apparently too small to be imaged via microscopy.[8] However, very recently Laurer and Winey[8] have succeeded in directly imaging ionic aggregates in Zn-neutralized (≅1 mol %) semicrystalline poly(ethylene-*co*-methacrylic acid). The Zn-enriched aggregates were found to be nearly spherical and roughly 26 Å in diameter, and Zn-aggregation numbers were estimated to be in the broad range of 5−80 depending on the assumed aggregate composition.

Theoretically, major progress has been made over the past two decades in describing microphase separation of nonpolar diblock copolymers based on a variety of different methods.[15,19−23] In contrast, associating polymers in general, and ionomers in particular, are not nearly as well understood. For ionomers, highly phenomenological models, often containing many adjustable parameters (deduced by fitting to small-angle scattering data), largely remain the state-of-the-art.[1,18,24] Some reasons for the modest theoretical progress include the following: (a) the presence of very strong ($\epsilon_{BB} \gg k_BT$) attractive forces between the small minority species, (b) microdomains of dimensions not vast compared to monomer size and other local chemical length scales, (c) large surface-to-volume ratio of sticky group clusters, (d) highly asymmetric composition of A and B groups in the heteropolymer, and (e) the lack of long-range order. The first reason has almost entirely precluded computer simulation studies of concentrated systems due to equilibration difficulties.[25] Considerations a−d also may severely limit the utility of coarse-grained polymer physics type approaches based on the incompressible random phase approximation (RPA), field theoretic and scaling methods, and/or strong segregation analytic analysis. Lack of microscopic theories is one reason for the remaining fundamental questions and debate concerning the origin and interpretation of small-angle X-ray scattering measurements of microdomains in ionomer melts. An interesting recent qualitative scaling-type statistical thermodynamic analysis for ionomers has exploited analogies to highly asymmetric diblock and triblock copolymers in a "super strong segregation limit" (SSSL).[26] However, quantitative predictions are lacking, and the measurable collective scattering structure factors and real space pair correlation functions are not obtainable by this approach. Field theoretic attempts to go beyond the RPA to treat the difficult problem of strongly attractive interactions remain largely at the formal level.[27,28]

The goal of this paper is to propose and apply a microscopic liquid state integral equation theory approach for strongly associating polymer melts. It is a direct generalization of the "polymer reference interaction site model" (PRISM) theory of Curro and Schweizer and builds on recent successful applications to self-assembling diblock copolymer melts and solutions.[19,29] PRISM is the polymeric generalization of the RISM theory of Chandler and Andersen for fluids of small rigid molecules.[30] We believe that physical considerations a−e discussed above make a liquid state theory approach well suited for describing microphase separation into small, highly correlated clusters or multiplets. The influence of chain connectivity and intermolecular excluded volume constraints on microdomain structure and self-assembly is accounted for on all length scales by PRISM theory, in strong contrast to simple RPA type approaches. Moreover, the influence of variable global architecture, chemically specific features such as A and B monomer size and backbone semiflexibility, and the form and range of intermolecular potentials can all be naturally taken into account. We shall focus in this initial paper solely on meltlike conditions where nonideal conformational effects (e.g., chain stretching) are minimized.

We anticipate that the liquid state approach will be valuable for describing weak and intermediate levels of segregation. However, accurate treatment of strong, or "super-strong", segregation may not be feasible for both practical numerical reasons and conceptual considerations associated with the difficulty of integral equation theories to support very sharp interfaces.[31] Thus, the PRISM approach would appear to be complementary to the recent scaling/strong segregation theories.[26] However, it is important to realize that the definition of weak, intermediate, strong, and super-strong segregation regimes is far less clear for associating heteropolymers compared to diblock copolymers,[15] and which regime a specific experimental material may fall into does not seem presently possible to a priori predict.

Of fundamental interest in associating polymers is their connectivity properties such as gelation and cluster distribution. Such connectivity properties can potentially be explicitly addressed using approximate liquid state theory methods to compute "pair-connectedness" type correlation functions, but this topic is beyond the scope of our present investigation. We also do not consider truly long-range-ordered microphase-separated states. This requires a theory for the free energy of the ordered phase and the order−disorder phase transition. However, in most real associating polymer materials (e.g., ionomers) spatially long-range order is not present. The microphase-segregated structure of interest emerges continuously in a cooling experiment, and the isotropic fluid is locally segregated (clustered) with possibly very strong short-range order between microdomains. Liquid state theory is appropriate for describing this physical situation.

The goal of this paper is 2-fold. The first is to present the straightforward generalization of PRISM theory to a variety of (periodic) copolymer architectures; this is done in section II. The second is to explore via systematic numerical calculations its predictions for microdomain scale self-assembly as encoded in small-angle partial scattering structure factors. Section III presents results for telechelic and surfactant architectures, and multiblock copolymers are studied in section IV. Qualitative comparisons with experimental scattering data, and speculative comments regarding their possible connections with mechanical behavior, is the subject of section V. The paper concludes in section VI with a brief summary and discussion. Various technical aspects and extensions of the theory are the subject of three appendices. In the following companion paper we present our complementary results for *real space* correlation functions and various measures of physical clustering. Combining the real and Fourier space theoretical information, we construct a global picture of self-assembly, and contrast it with prior phenomenological models and experimental observations.

II. Theory

Both the chain model and polymer integral equation approach we employ are nearly standard and have been

discussed in depth in previous work.[19] Thus, we sketch only the essential elements. Since our primary interest is in ionomers, we discuss our model and results in the context of these materials.

A. Polymer Model. Consider a fluid of polymer chains each composed of N total sites at a molecular number density ρ. Each compositionally and degree of polymerization monodisperse heteropolymer has two chemically distinct spherical interactions sites, A and B, in alternating blocks along the chain. There are P_M blocks and N_M repeat units per block of species type M, and f_M is defined as the fraction of type M sites. The total number of species type M is $n_M = P_M N_M$.

A pair of sites of type M and M′ on different chains interact via a hard core repulsion corresponding to a distance of closest approach of $\sigma_{MM'} = (\sigma_M + \sigma_{M'})/2$. In this paper, we consider only the symmetric case of $\sigma_A = \sigma_B = \sigma$. Each site is envisioned as a cartoon model of a real monomer; as such, based on typical experimental molar volumes of ≅50−100 Å^3, $\sigma \cong 5-8$ Å, for ionomers of common interest such as polystyrene, polybutadiene, and polyisoprene. The strongly associating groups are labeled "B" sites and are modeled as interacting via a Lennard−Jones-like attraction for $r > \sigma$:

$$V_{BB}(r) = \epsilon_{BB}[(r/\sigma)^{-12} - 2(r/\sigma)^{-6}], \quad r \geq \sigma \qquad (2.1)$$

A positive dimensionless measure of the strength of the B group attractions is $\beta\epsilon_{BB}$, where $\beta = 1/k_B T$. Alternatively, a mean field ("bare") Flory χ-parameter can be defined as

$$\chi_0 = \rho_m \int d\vec{r}\ \beta V_{BB}(r) = (20\pi/9)\rho_m \sigma^3 \beta\epsilon_{BB} \qquad (2.2)$$

where $\rho_m = N\rho$ is the total site number density.

The dimensionless effective attractive energy parameter, $\beta\epsilon_{BB}$, is controlled by temperature and the chemical structure of the associating polymer system. Many factors enter, such as (i) the chemical nature of the acid (e.g., sulfonate or carboxylate), (ii) valency and ionic radius of the neutralizing metal cation (e.g., Na, K, Rb, Mg, Zn), (iii) dielectric constant of the polymer, (iv) strength of the ionic bond formed between acidic anion and metal cation, and (v) monomer shape defining local steric constraints on sticky group association. Consequently, $\beta\epsilon_{BB}$ can be varied over a wide range. Although difficult to precisely compute from first principles, estimates in the literature suggest $\beta\epsilon_{BB} \gg 1$ is easily realizable. For ethylene−sodium methacrylate ionomers (−COO^-Na^+ ion pair), Eisenberg estimates $\beta\epsilon_{BB} \cong 2-24$ at room temperature depending on various system-specific factors; *larger* values are expected for sulfonic acids.[14,16]

Of course, in real systems, there will also be attractive interactions between AA and AB sites. These could easily be numerically included in the present theory, but introduce two more material specific parameters in our compressible fluid model. For strongly associating polymers the AA and AB cohesive forces are primarily of weak dispersive origin (of order $k_B T$ or less), and hence much smaller than the strong BB attractive potential. Hence, we expect that inclusion of $V_{AA}(r)$ and $V_{AB}(r)$ attractive tails, especially at the high meltlike densities of present interest, will make little difference in our studies. Thus, for simplicity we have ignored them entirely. This is consistent with the standard idea in associating polymer fluids that self-assembly is driven by the very strong BB attractive interactions.

The elementary sites of our model are connected by rigid bonds of length $L = \sigma$ corresponding to the "tangent" bead model. Backbone semiflexibility is included by introducing a bond bending energy between three nearest neighbor sites according to the standard discrete Koyama model,[32] the technical details of which are briefly summarized in Appendix A. In this paper we choose the bond bending energy to be uniform along the chain, and of a magnitude corresponding to a chain persistence length of ($^4/_3$)σ. The latter value implies a modest chain "aspect ratio" of $^4/_3$, typical of many polyolefins, polydienes, and vinyl polymers.[33] The reduced site density, $\rho_m\sigma^3$, or equivalently a total monomer packing fraction, $\eta = (\pi/6)\rho_m\sigma^3$, is chosen such that in the athermal homopolymer limit ($\beta\epsilon_{BB} \to 0$) the dimensionless reduced compressibility is a value typical[33] for a concentrated solution or dense melt, $k_B T \rho_m \kappa \cong 0.2-0.4$. For the above semiflexible chain model, this criterion implies $\eta \cong 0.3-0.4$.

The semiflexible chain is a model of intermediate level realism. Although it neglects angstrom scale chemical structural features present in real polymers, this model has been shown to be very useful in understanding several properties of a homologous series of melts such as the polyolefins.[29,31,33] It also is a model of sufficient simplicity that many chain dense fluid computer simulations may be feasible soon. Since the fundamental aspects of self-assembly of strongly associating polymer fluids seem to be quite general,[1] we believe the model is adequate for an initial theoretical study. It is worth pointing out that this chain model is the most realistic considered to date either theoretically or via computer simulation. Schematic pictures of the chain architectures considered in this work are shown in Figure 1.

B. Multiblock Copolymer PRISM Theory. We follow the general analysis of David and Schweizer[19] for block copolymers. For practical tractability reasons, the standard pre-averaging approximation[29] is adopted corresponding to treating all sites of the same type (A or B) as symmetry-equivalent with regards to *inter*molecular interactions. The corresponding 2 × 2 matrix of PRISM integral equations in Fourier space is then given by[19]

$$\hat{\mathbf{H}} = [\mathbf{1} - \hat{\Omega}\hat{\mathbf{C}}]^{-1}\hat{\Omega}\hat{\mathbf{C}}\hat{\Omega} \qquad (2.3)$$

where $\hat{H}_{MM'}(k) = \rho_M \rho_{M'} \hat{h}_{MM'}(k)$, $1 + h_{MM'}(r) = g_{MM'}(r)$ is the *inter*molecular site−site radial distribution function, $\hat{\Omega}_{MM'}(k) = \rho \sum_{\alpha=1}^{N_M} \sum_{\gamma=1}^{N_M}{}' \hat{\omega}_{\alpha M \gamma M'}(k)$ are the species-averaged partial *intra*molecular structure factors where $\omega_{\alpha M \gamma M'}(r)$ is the normalized probability distribution function for finding site a of species M a distance r from site γ of species M′, $\hat{C}_{MM'}(k)$ are the site−site *inter*molecular direct correlation functions, and ρ_M is the site number density of species M. For multiblock copolymers of the form (B−A)$_P$-B, the diagonal partial structure factors include intrablock and cross-block contributions and are given by

$$\hat{\omega}_{MM}(k) = \frac{1}{P_M N_M}\Big[\sum_{\alpha,\gamma=1}^{N_M} P_M \hat{\omega}_{\alpha,\gamma}(k) + 2\sum_{\nu=1}^{P_M-1}(P_M-1)\hat{\omega}^{\nu-1}_{1,N_M}(k)\hat{\omega}^{\nu}_{1,N_{M'}}(k)\sum_{\alpha,\gamma=1}^{N_M}\hat{\omega}_{\alpha,N_M}(k)\hat{\omega}_{1,\gamma}(k)\Big] \quad (2.4)$$

The off-diagonal counterpart is

$$\hat{\omega}_{AB}(k) = \frac{1}{N}\Big[2\sum_{\nu=0}^{P_A-1}(P_A-\nu)\hat{\omega}^{\nu}_{1,N_A}(k)\hat{\omega}^{\nu}_{1,N_B}(k)\sum_{\alpha=1}^{N_A}\hat{\omega}_{1,\alpha}(k)\sum_{\gamma=1}^{N_B}\hat{\omega}_{1,\gamma}(k)\Big] \quad (2.5)$$

The normalization convention is $\hat{\omega}_{MM}(k=0) = n_M$ and $\omega_{AB}(k=0) = n_A n_B/N$. The diblock copolymer case[19] follows from setting $P_M = 1$ and dropping the second term in eq 2.4. These intramolecular partial structure factors are computed based on the Koyama semiflexible chain model[29,32] invoking "Flory ideality" in the sense that the conformational statistics are taken to be unaffected by thermodynamic state variables. This is reasonable at the high meltlike densities of interest in this work. The few available direct experimental measurements of conformation for associating ionomer melts suggests very little, if any, chain stretching accompanies the microphase separation process.[34] More sophisticated "self-consistent" versions of PRISM theory exist[29] to allow for conformational perturbation but will not be utilized in this work.

Formally, the intermolecular pair correlations have the same form as for the diblock case:[19]

$$\hat{\Lambda}\hat{h}_{AA} = \hat{\omega}_{AA}{}^2\hat{C}_{AA} + \frac{\hat{\omega}_{AB}{}^2\hat{C}_{BB}}{f_{AA}{}^2} + \frac{2\hat{\omega}_{AA}\hat{\omega}_{AB}\hat{C}_{AB}}{f_A} - \rho_B\hat{\omega}_{AA}\delta\hat{\omega}\delta\hat{C} \quad (2.6)$$

$$\hat{\Lambda}\hat{h}_{AB} = \left(\hat{\omega}_{AA}\hat{\omega}_{BB} + \frac{\hat{\omega}_{AB}{}^2}{f_A f_B}\right)\hat{C}_{AB} + \hat{\omega}_{AB}\left(\frac{\hat{\omega}_{AA}\hat{C}_{AA}}{f_B} + \frac{\hat{\omega}_{BB}\hat{C}_{BB}}{f_A}\right) - \rho_m\hat{\omega}_{AB}\delta\hat{\omega}\delta\hat{C} \quad (2.7)$$

where

$$\hat{\Lambda}(k) = 1 - \rho_A\hat{\omega}_{AA}\hat{C}_{AA} - \rho_B\hat{\omega}_{BB}\hat{C}_{BB} - 2\rho_m\hat{\omega}_{AB}\hat{C}_{AB} + \rho_A\rho_B\delta\hat{\omega}\delta\hat{C} \quad (2.8)$$

$$\delta\hat{\omega}(k) = \hat{\omega}_{AA}(k)\hat{\omega}_{BB}(k) - f_A{}^{-1} f_B{}^{-1}\hat{\omega}_{AB}(k)^2 \quad (2.9)$$

$$\delta\hat{C}(k) = \hat{C}_{AA}(k)\hat{C}_{BB}(k) - \hat{C}_{AB}{}^2(k) \quad (2.10)$$

and ρ_m is the total site number density. The corresponding partial total structure factors, or Fourier transformed density−density fluctuation correlation functions, follow from the matrix relation $\hat{\mathbf{S}} = [\mathbf{1} - \hat{\Omega}\hat{\mathbf{C}}]^{-1}\hat{\Omega}$ yielding[19]

$$\hat{S}_{AA}(k) = [\rho_A\hat{\omega}_{AA}(1 - \rho_B\hat{\omega}_{BB}\hat{C}_{BB}) + \rho_m{}^2\hat{\omega}_{AB}{}^2\hat{C}_{BB}]/\hat{\Lambda} \quad (2.11)$$

$$\hat{S}_{AB}(k) = [\rho_m\hat{\omega}_{AB}(1 - \rho_m\hat{\omega}_{AB}\hat{C}_{AB}) + \rho_A\rho_B\hat{\omega}_{AA}\hat{\omega}_{BB}\hat{C}_{AB}]/\hat{\Lambda} \quad (2.12)$$

$\hat{S}_{BB}(k)$ is obtained from eq 2.11 by interchanging the A and B labels.

A "closure approximation" is required to complete the theory. For multicomponent polymer blends and diblock copolymers, a family of novel "molecular closures" have been proposed by Schweizer and Yethiraj,[35] and successfully applied in the past.[29] For site−site potentials of a hard core plus $V_{MM'}(r)$ tail, the molecular closures have the general form

$$[\Omega^*\mathbf{C}^*\Omega]_{MM'}(r) = \{\Omega^*[\mathbf{C}^{(0)} + \Delta\mathbf{C}]^*\Omega\}_{MM'}(r), \quad r > \sigma_{MM'} \quad (2.13)$$

where the asterisks denote convolutions in r-space. $C^{(0)}_{MM'}(r)$ are the set of site−site direct correlation functions for a hard core (athermal) reference fluid, while the attractive tail potentials enter via an approximation for $\Delta C_{MM'}(r)$. The closure approximation is supplemented by the exact core impenetrability constraint

$$g_{MM'}(r) = 0, \quad r < \sigma_{MM'} \quad (2.14)$$

The properties of the hard core reference fluid are determined by using the standard, and quite accurate,[29] site−site Percus−Yevick (PY) closure[30]

$$C^{(0)}_{MM'}(r) = 0, \quad r > \sigma_{MM'}, \qquad h^{(0)}_{MM'}(r) = -1, \quad r < \sigma_{MM'} \quad (2.15)$$

As discussed in great detail elsewhere,[19,29,35] several distinct approximations have been proposed for $\Delta C_{MM'}(r)$ in eq 2.13 and studied for different multicomponent polymer problems. Non-mean-field concentration fluctuation effects have been successfully treated in both symmetric polymer mixtures and diblock copolymers based on the reference−molecular Percus−Yevick (R−MPY) closure defined as

$$\Delta C_{MM'}(r) \cong -[1 - e^{-\beta V_{MM'}(r)}]g_{MM'}(r) \quad (2.16)$$

Much progress has also been made based on a conceptually (and from a numerical implementation viewpoint) simpler "high-temperature approximation (HTA)" version of this closure

$$\Delta C_{MM'}(r) \cong -[1 - e^{-\beta V_{MM'}(r)}]g^{(0)}_{MM'}(r), \quad \text{R−MPY/HTA} \quad (2.17)$$

and its linearized counterpart

$$\Delta C_{MM'}(r) \cong -\beta V_{MM'}(r) g^{(0)}_{MM'}(r) \quad (2.18)$$

where the superscript zero denotes the athermal reference fluid. These two HTA closures are equivalent for weak tail potentials, $-\beta V_{MM'}(r) < 1$, as is often the relevant situation for nonpolar blends and block copolymer liquids. However, for strongly associating polymers, the weak coupling limit will not apply literally, and differences between PRISM theory predictions based on eqs 2.16−2.18 are to be expected. Both of the HTA closures can be viewed as a thermodynamic perturbation approximation at the level of the renormalized or effective potentials.[29,35]

A priori, it is difficult to know which of the above molecular closures will be most accurate; in numerical work, the full R−MPY approximation is much harder

to work with. Since the linearized R−MPY/HTA has been successfully applied to many problems involving nonpolar polymer blends and diblock copolymers,[19,29,35] and also the liquid−vapor transition of homopolymer fluids,[36] we shall adopt it for the majority of our initial numerical studies. This closure also has the advantage of allowing analytic results to be derived for simplified chain models, and direct contact with other theoretical approaches such as the RPA can be made. To explore the influence of closure approximation for systems with strong attractive forces, we have performed a limited set of calculations with the nonlinear version eq 2.17; the results are discussed in Appendix C. We do caution that the detailed temperature dependencies of various structural and thermodynamic quantities will be sensitive to the closure employed. Determination of the most accurate thermal closure approximation will require comparison with benchmark computer simulation studies, which to date do not exist. Thus, throughout the presentation of our main results based on eq 2.18 we indicate which trends are expected to be generally valid and which are tied closely to the specific approximation adopted to treat the difficult problem of strong attractive forces.

The PRISM equations with the appropriate closures were solved numerically using standard Picard iteration methods described previously.[19]

III. Telechelics

The telechelic architecture is essentially a "mini-triblock", and we consider first the simplest $N_B = 1$ "end-capped" form corresponding to a single associating B group on each chain end. Attracting group fractions of $f_B = 1$, 2, 3, 5, and 8% have been studied, corresponding to total degrees of polymerization of N ranging from 200 to 25. The total site packing fraction is fixed at a concentrated solution or meltlike value of $\eta = 0.3$ for which $\hat{S}(0) \cong 0.25$. The choice of these model systems is motivated by their relevance to several experimental studies of telechelic melts,[2−4] and the possibility that melts composed of chains of such modest size and packing fraction might be computer simulated soon.

To gain insight concerning the influence of controllable features such as sequence and sticky group block size, we also study several other models: (a) $N_B = 3$ telechelics, (b) $N_B = 3$ (and a few $N_B = 1$ and 5) regular multiblocks, and (c) "surfactants", or monotelechelics. For these other cases, we shall present additional figures only if they illustrate how different molecular architecture can significantly change the microdomain scale structure.

A. Characteristic Temperatures and Fluctuation Stabilization. Self-assembly in most associating polymer melts does not correspond to a true thermodynamic phase transition with long-range order. Instead, there is a strong physical association of the sticky minority groups into small clusters or multiplets, and such objects are spatially correlated. This aggregation process is directly reflected in the dimensionless partial static structure factor of the associating groups, $\hat{S}_{BB}(k)/\rho_B$. Because of electron density contrast associated with a metal cation, small-angle X-ray scattering (SAXS) experiments on ionomer melts are often dominated by this quantity, which exhibits a small wave vector "ionomer peak" associated with microphase separation.[1] Moreover, the scattering from the majority phase is not expected to be strongly changed from that appropriate

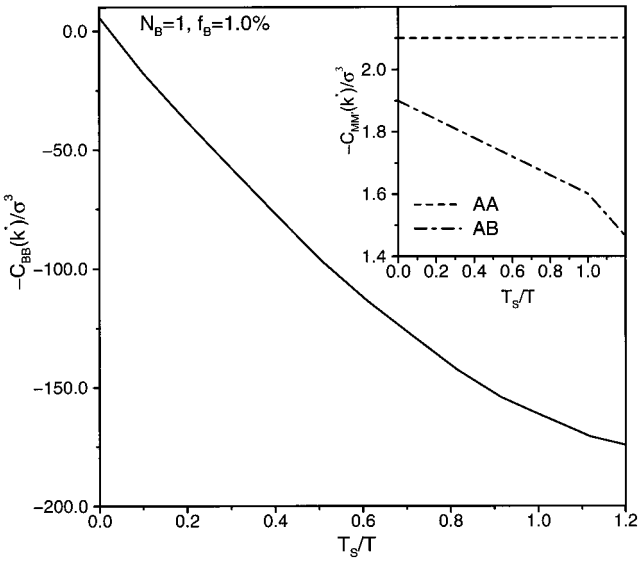

Figure 2. Wave vector dependent direct correlation function evaluated at $k = k^*$ as a function of reduced inverse temperature for the minority B species of a $N_B = 1$, $f_B = 1\%$ telechelic melt. Inset: The corresponding quantity for the majority species (AA) and AB cross correlation.

in the athermal limit, i.e., a nearly incompressible homopolymer melt. An indication that this is true is given in Figure 2 which shows an example for a telechelic melt of the integrated strength of the effective intermolecular potentials (direct correlations, $-k_BTC_{MM'}(r)$) as a function of reduced inverse temperature (as described below). Note that the BB effective interactions are extremely large, and upon cooling are dominated by the attractive force. On the other hand, the AA majority interaction is repulsive and virtually temperature independent, while the AB interaction strength is repulsive but weakly reduced due to the clustering of B monomers. These features for the direct correlation functions translate directly into the predicted behavior for the collective structure factors, resulting in the qualitative behavior described above.

Experimentalists often present small-angle scattering data with suitable "background subtractions" to try and isolate the scattering associated with ionic group self-assembly.[1−14] In the small-angle regime, we find that at all lower temperatures, T, of interest

$$\hat{S}_{BB}(k;T) \approx \hat{S}_{BB}(k;T) - \hat{S}_{BB}(k;T\to\infty) \approx \hat{S}_{TOT}(k;T) - \hat{S}_{TOT}(k;T\to\infty) \quad (3.1)$$

where $\hat{S}_{TOT}(k)$ is the total scattering intensity. Thus, various "background subtraction" procedures applied to our theoretical information makes little or no difference. Thus, we will focus primarily on $\hat{S}_{BB}(k;T)$ as an indicator of both self-assembly and SAXS profiles. We first present results for the collective BB scattering, and analyze them in the framework employed for thermally driven self-assembling diblock copolymer melts.[15,19]

The degree of order can be characterized by the intensity of the small-angle scattering maximum at $k = k^*$, normalized by its value in the unassociated, athermal homopolymer melt ($\chi_0 \propto \beta\epsilon_{BB} \to 0$): $\hat{S}_{BB}(k^*)/\hat{S}_{BB}(k^*)|_{\chi\to 0}$. A schematic plot of the inverse of this quantity vs inverse temperature is shown in Figure 3. As the fluid is cooled and microdomains are forming, the peak scattering intensity grows in a "mean field" manner[20] corresponding to the linear portion of the

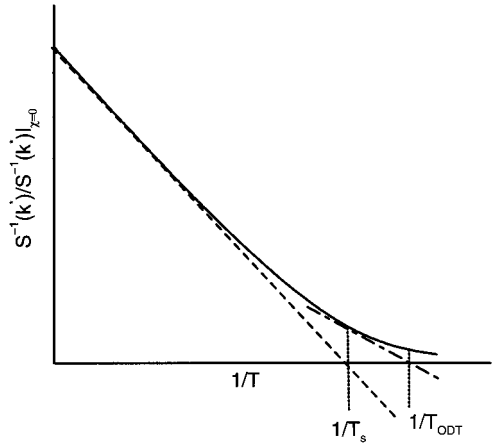

Figure 3. Schematic of the inverse reduced peak intensity vs inverse reduced temperature cooling curve which shows how the apparent spinodal (T_s) and ODT (T_{ODT}) temperatures are defined based on extrapolation.

curve in Figure 3. Extrapolation of this linear portion to divergent intensity defines an "apparent mean field spinodal temperature", T_s. However, no divergence actually occurs because there is no second-order phase transition.[19,21] Rather, "fluctuation processes" enter which arrest the unbounded growth of the scattering intensity, and this shows up as the curved, or nonlinear, portion of the curve in Figure 3. A lower temperature, T_{ODT}, which characterizes the strength of this fluctuation stabilization process can be graphically extracted[19] as shown in Figure 3. For diblock copolymer melts, this temperature has been shown to correlate very well with the width of the fluctuation regime ($\propto N^{-1/3}$) and the location of the true weakly first-order phase transitions found in such systems.[19] We shall adopt T_s and T_{ODT} as two system-dependent measures of the onset of significant microdomain/cluster formation and a much stronger intermediate level segregation, respectively. Whether such temperatures are experimentally accessible will depend on the specific system via the absolute magnitude of $\beta\epsilon_{BB}$.

Examples of the normalized peak intensity vs normalized inverse temperature cooling curves are shown in Figure 4. The plots begin only at $T_s/T = 0.2$ because at higher temperatures the $N_B = 1$ telechelics melts do not exhibit any low-angle scattering peak in $\hat{S}_{BB}(k)$. This lack of discernible microdomain structure at high temperatures is in contrast with the behavior of diblock copolymers where a "correlation hole" peak always occurs for simple chain connectivity and low melt compressibility reasons.[15,20] The nonlinear shape, or "fluctuation regime", of these curves clearly depends on sticky group composition and block length, and also global architecture. In all cases, the degree of nonlinear "bending over" is stronger relative to that in diblock copolymers[19,21] since the physical origin of this effect within PRISM theory is a finite size coupling of the physical clustering of like species on the microdomain and monomer length scales.[19] The latter are much closer for the associating telechelics and multiblocks than for large diblocks. As expected, the degree of nonlinearity increases as the associating group concentration f_B increases (N decreases) at fixed N_B or for smaller B block size N_B (smaller microdomains) at fixed f_B. This nonlinearity can be further quantified via the ratio T_s/T_{ODT}, which is typically $\cong$1.3 (e.g., for $N_B = 1$ telechelics it varies from 1.3 to 1.36 for $f_B = 1-8\%$, and it is very

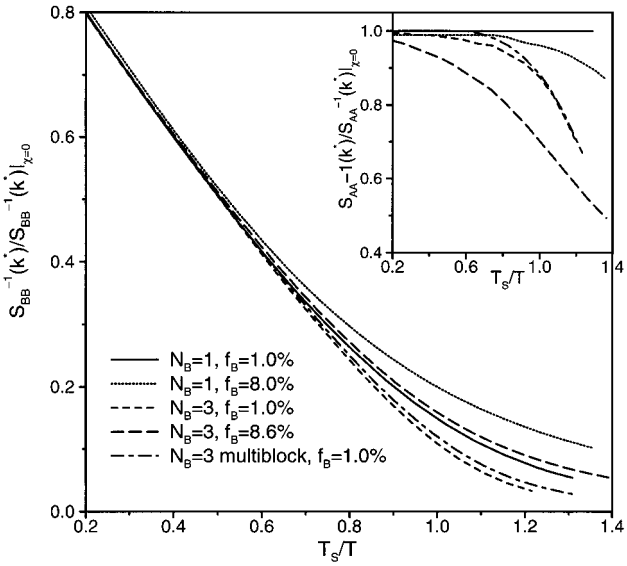

Figure 4. Inverse peak BB scattering intensity normalized by its athermal value as a function of reduced inverse temperature for $N_B = 1$, 3 telechelics and a $N_B = 3$ multiblock at various indicated B group fractions f_B. Inset: Same quantity but for the AA majority species. For all cases the BB scattering function has been employed to determine the apparent spinodal temperature.

similar for $N_B = 3$). If the peak intensity saturated at low temperatures, one could identify a globally isotropic but limiting "ground state like", or "super strong segregation", structure. Such behavior has been found within PRISM theory for diblock copolymers,[19] but it is inaccessible for the present cases due to commonly encountered low-temperature convergence problems of the numerical algorithm used to solve the nonlinear integral equations.[37]

The peak intensity normalized by the sticky group concentration variable, $\hat{S}_{BB}(k^*)/\rho_B$, is a natural dimensionless "order parameter". A reasonable collapse (not shown) of all the $N_B = 1$ data for the $f_B = 1$,3 and 8% cases is found when the natural logarithm of this order parameter is plotted vs the quantity $(\beta\epsilon_{BB})f_B^{2/3}$, implying an exponential growth law over a range of temperature where the dimensionless intensity increase by more than 1 order of magnitude.

PRISM theory also provides the other two scattering functions, $\hat{S}_{AA}(k)$ and $\hat{S}_{AB}(k)$. For all cases studied, these behave very differently than $\hat{S}_{BB}(k)$, and strongly deviate from incompressible RPA law of $\hat{S}_{AA}(k) = \hat{S}_{BB}(k) = -\hat{S}_{AB}(k)$. Examples are shown in the inset of Figure 4 for the majority component peak intensity. For the $N_B = 1$ telechelics, *no* low-angle peak in $\hat{S}_{AA}(k)$ essentially *ever* emerges at any temperature studied if $f_B < 8\%$. For longer B block lengths, a weak low-angle peak develops with a peak intensity that shows *qualitatively different* dependence on cooling than for $\hat{S}_{BB}(k^*)$. This behavior might be experimentally measured by small-angle neutron scattering if the A monomers are deuterium labeled.

The apparent spinodal temperatures as a function of associating group concentration are shown in Figure 5. Comparison is also made with the predictions of incompressible RPA theory which is discussed in Appendix B. The RPA ignores the influence of excluded volume packing constraints on the tendency of the B group attractions to induce microdomain formation, and hence predicts a literal spinodal at $T_{s,RPA}$ with divergent

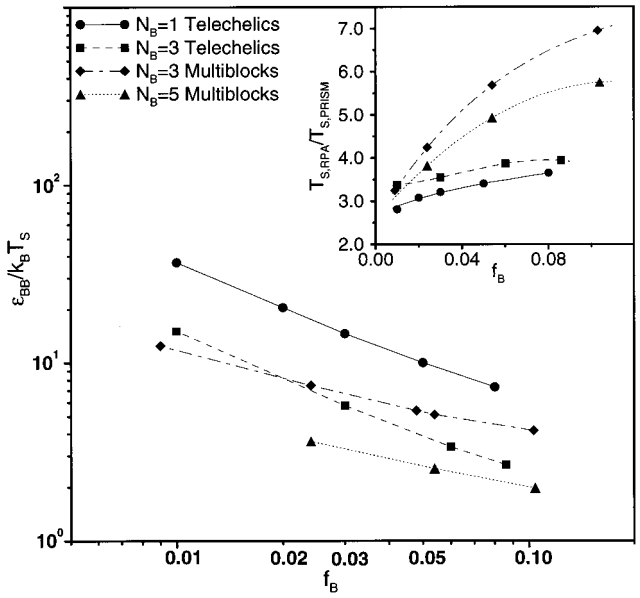

Figure 5. Logarithmic plot of the dimensionless inverse apparent spinodal temperature as a function of sticky group fraction for $N_B = 1$, 3 telechelics and $N_B = 3$, 5 multiblock architectures. In each case the spinodal temperature scales as a power law, $T_s \propto f_B^{\nu}$, where $\nu = 0.78$, 0.77, 0.48, 0.41 for the $N_B = 1$, 3 telechelic and $N_B = 3,5$ multiblock, respectively. Inset: Comparison of incompressible RPA predictions of the spinodal temperature with PRISM results.

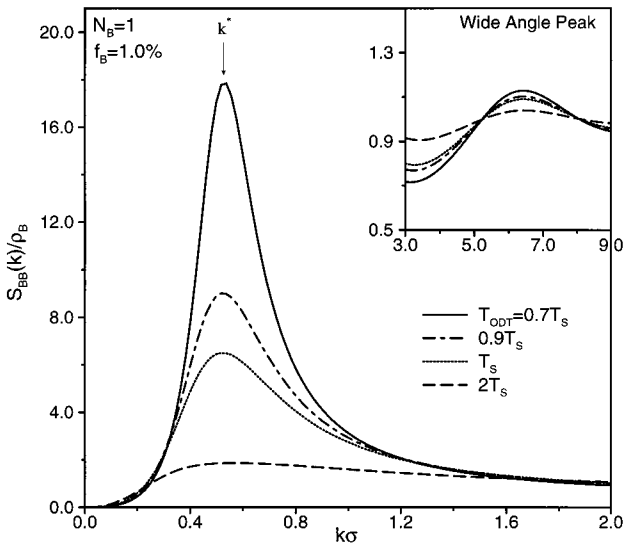

Figure 6. Dimensionless low wave vector scattering profile for the minority species at various indicated temperatures for the $f_B = 1\%$, $N_B = 1$ telechelic. Note that even halfway to the spinodal temperature the scattering peak is very broad and a peak is barely discernible. Inset: Wide-angle regime for the same system.

scattering intensity at k^*. For this reason, it is expected on general grounds to significantly overestimate the tendency for physical clustering and the magnitude of T_s. This expectation is borne out in Figure 5 where $T_{s,RPA}/T_{s,PRISM}$ is seen to vary between 2.5 and 7; moreover, it is clear that differences increase systematically with larger associating group concentration and/or block length. In all cases, good effective power law dependencies of the PRISM theory *apparent* spinodal temperature on f_B are found, and the exponents are listed in the figure caption. The telechelics exhibit the strongest dependence of T_s on sticky group fraction, in a manner which is nearly independent of block length N_B, and only slightly weaker than the RPA prediction of $T_s \propto f_B^{0.8}$.

For the $N_B = 1$ telechelics, the absolute magnitude of ϵ_{BB} varies over the range of $10-40 k_B T_s$. Although very large, if one identifies T_s as room temperature, then such values are seemingly not unphysical based on the estimates discussed in section IIB. As discussed in Appendix C, the precise numerical values of this energy are weakly sensitive to the detailed spatial form of the associating group interaction potential, and rather strongly sensitive to the closure approximation. Significantly smaller values of $\epsilon_{BB}/k_B T_s$ are found based on the nonlinear R−MPY/HTA closure which all fall well within the crude estimates of section IIB.

B. Cluster Scattering Profiles. An example of the temperature dependence of the associating group low-angle scattering function is shown in Figure 6 for a 1% telechelic. As the fluid is cooled, a weak low-angle peak eventually emerges around $T \cong T_s/2$, and for $T < T_s$ it grows very strongly in intensity, narrows dramatically, and shifts weakly to smaller wave vectors. There is no excess scattering at small wave vectors, or "low-angle upturn", which is now generally accepted as a nonequilibrium effect.[1] The characteristic microdomain period is a collective liquid property defined as $D = 2\pi/k^* \cong 12\sigma$, which is smaller than the single chain mean square end-to-end distance of $R_{EE} \cong 16\sigma$.

The corresponding wide-angle peak associated with BB monomer−monomer local correlations on a length scale $\sigma \cong 10$ times smaller than D is shown in the inset. Its absolute intensity is small compared with the low-angle microdomain peak. Decreasing temperature enhances the intensity and sharpness of the wide-angle peak. Since this feature controls segmental scale packing, it strongly influences local dynamics and the glass transition. Microscopic theories of the supercooled liquids and the glass transition predict that modest enhancements of the wide-angle scattering features are able to greatly slow local dynamics.[38] Thus, the enhancement of B monomer local packing or cage constraints which emerge upon microdomain formation may result in a larger glass transition temperature, an effect observed experimentally.[12,13] The influence of microdomain formation on wide-angle scattering becomes progressively *stronger* (not shown) as the ratio D/σ is reduced by decreasing chain length and/or increasing associating group concentration, and hence, it would be expected to further slow local dynamics relative to the parent homopolymer liquid, a trend also consistent with mechanical experiments.[1]

An example of the influence of associating group concentration (at *fixed* absolute T) on the cluster scattering profile is shown in Figure 7. The microdomain peak intensity is strongly enhanced, shifts to higher wave vector, and strongly narrows as f_B (microdomain period) increases (decreases).

At low temperature the shape of the scattering curves in Figures 6 and 7 neither are Lorenztian (as often found for diblock copolymers near the ODT)[39] nor agree with the RPA form (see Appendix B). An example which makes this point is given in Figure 8 for $N_B = 1$ telechelics at T_{ODT}. For purposes of comparison, the scattering curves have been aligned horizontally (via the reduced variable k/k^*) and vertically normalized to a common peak intensity (χ in the RPA expression was adjusted such that peak intensities agree). Clearly, the RPA structure factor is much broader, and becomes in

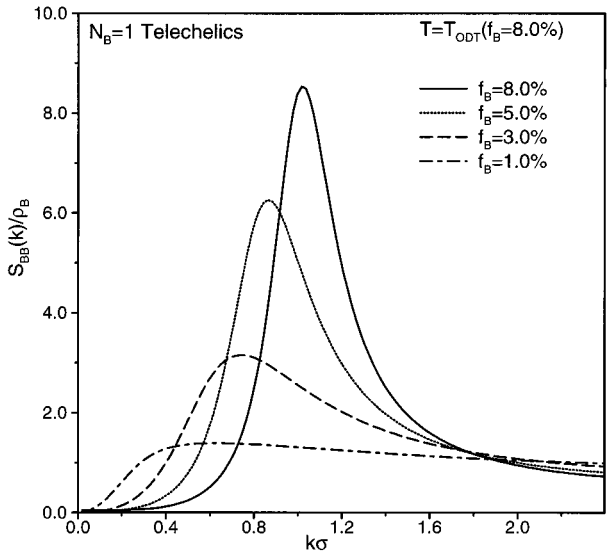

Figure 7. Dimensionless low wave vector scattering profile for the minority B species at a constant absolute temperature of $T = T_{ODT}$ ($f_B = 8\%$) for $N_B = 1$ telechelics.

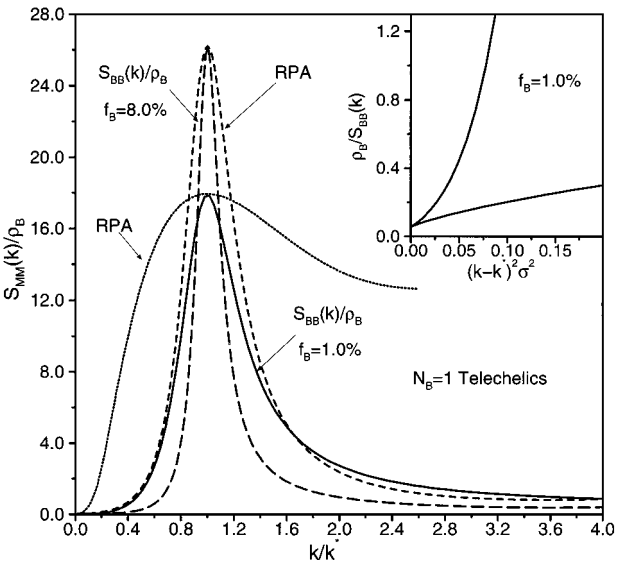

Figure 8. Comparison of the RPA structure factor to the analogous PRISM result for the low wave vector dimensionless minority species scattering function of $N_B = 1$ telechelics with $f_B = 1\%$ and 8%. Inset: PRISM results for the $f_B = 1.0\%$ case plotted in a format where straight line behavior would imply a Lorenztian line shape. The upper (lower) curve corresponds to the $k < k^*$ ($k > k^*$) part.

worse agreement with PRISM for the higher compositionally asymmetric telechelic. The inset shows the PRISM scattering curve is also not well described by a symmetrical Lorenztian function even close to the peak.

The shape of the scattering curve predicted by PRISM theory can be further characterized by analyzing it in terms of the standard Porod plots employed by experimentalists.[40] Low-temperature examples are shown in Figure 9. Recall that horizontal behavior in such a plot corresponds to the sharp interface Porod law of $\hat{S}_{BB}(k) \propto k^{-4}$, and "negative deviations" ($\hat{S}_{BB}(k) \propto k^{-4-b}$ with $b > 0$) contain information to estimate the interfacial width, W, separating A-rich and B-rich microdomains.[40] The Porodlike behavior seen in Figure 9 suggests that rather sharply defined, but small, B microdomains are being predicted by the theory in the T_{ODT} temperature region. For all telechelics *and* multiblocks studied (N_B

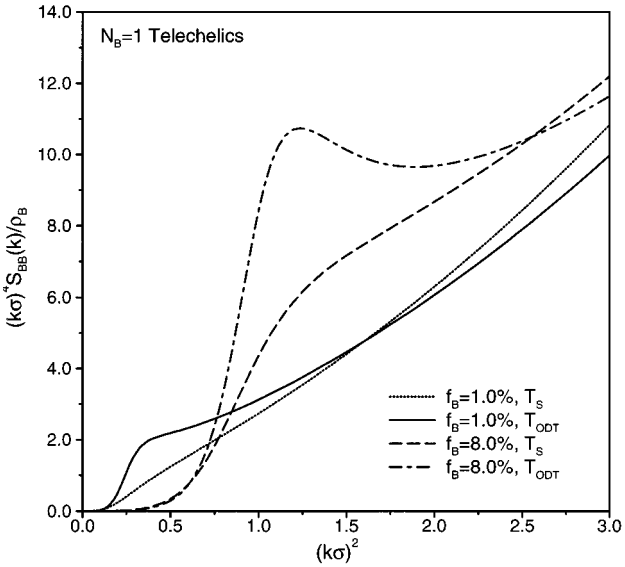

Figure 9. Porod plot for $N_B = 1$ telechelics and $f_B = 1$ and 8% at the apparent spinodal temperature and ODT. Note that, at the spinodal, despite the presence of a strong small-angle peak in $\hat{S}_{BB}(k)$, there is little evidence of a sharp interface in the Porod sense.

= 1 and 3), near T_{ODT}, an interfacial width of $W \cong 0.1-0.2\sigma$ is obtained based on standard analysis equations.[40] This corresponds to an absolute value of the order of 1 Å. Such a remarkably small value is qualitatively consistent with experimental attempts to measure narrow interfaces via a Porod analysis.[2,3]

We now analyze more carefully the temperature and associating group concentration dependencies of two primary collective BB scattering profile features: the peak scattering wave vector, k^*, or microdomain period $D = 2\pi/k^*$, and the profile fullwidth at half-maximum (fwhm), $\Delta k_{1/2}$. The size of the latter is a measure of the distribution in microdomain periods, and hence the degree of order in the fluid, and is expected to be *inversely* correlated with the peak scattering intensity $\hat{S}_{BB}(k^*)$. Alternatively, $\Delta k_{1/2}$ can be interpreted as a measure of how spatially correlated different B microdomains are, and in this spirit, we define a "coherence length scale" as $\xi_{coh} = 2\pi/\Delta k_{1/2}$. The inset of Figure 10 shows that upon cooling the microdomain period increases significantly and saturates at a limiting value around the spinodal temperature. Recall this temperature dependence is a *collective many chain effect* since the conformation of individual chains is fixed to be ideal and T-independent. Arrows indicate the values of $2\pi/R_{EE}$. We find that $R_{EE}/D = 1.51$, 1.22, 1.05 for $f_B = 1$, 3, 8%, thereby showing that the limiting microdomain period is smaller than the end-to-end distance of single chains, much more so as the chain length (associating group concentration) increases (decreases). Although the precise temperature dependence of k^* may be closure approximation dependent, reduction with cooling and saturation at low temperatures are generic features of PRISM theory for conformationally ideal chain models.

Thus, the physical picture emerges that the separation between nearest neighbor microdomains of small clusters ("multiplets") of B monomers is smaller than R_{EE}, and hence the two ends of a particular telechelic chain do not lie in nearest neighbor multiplets. This conclusion is reinforced by the log−log plot in the main part of Figure 10. The limiting low-temperature values of k^* follow the power law, $k^* \propto f_B^{0.31} \propto N^{-0.31}$, much

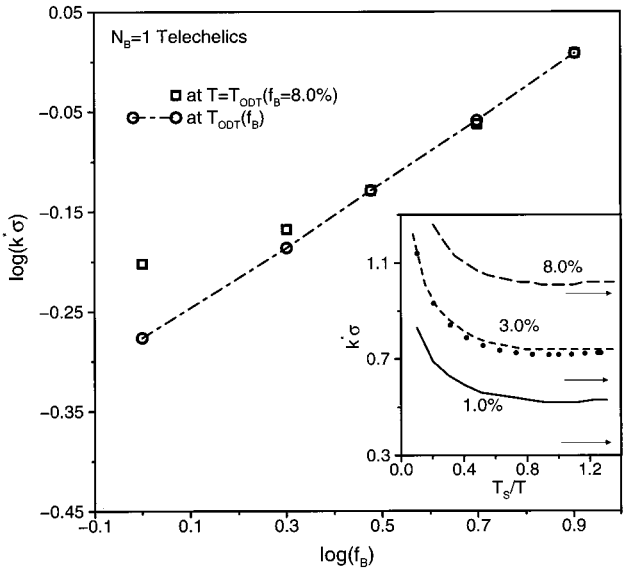

Figure 10. Dimensionless peak wave vector of $\hat{S}_{BB}(k)$ for $N_B = 1$ telechelics at the ODT and at a constant absolute temperature of $T = T_{ODT}$ ($f_B = 8\%$) as a function of sticky group composition. Inset: Same quantity as a function of reduced inverse temperature for three values of f_B. Note that k^* saturates near the spinodal. The arrows immediately below each curve indicate the corresponding value of $2\pi\sigma/R_{EE}$; in all cases $2\pi/R_{EE} < k^*$. The solid circles indicate results for a $N_B = 1$, $f_B = 1\%$ multiblock copolymer melt.

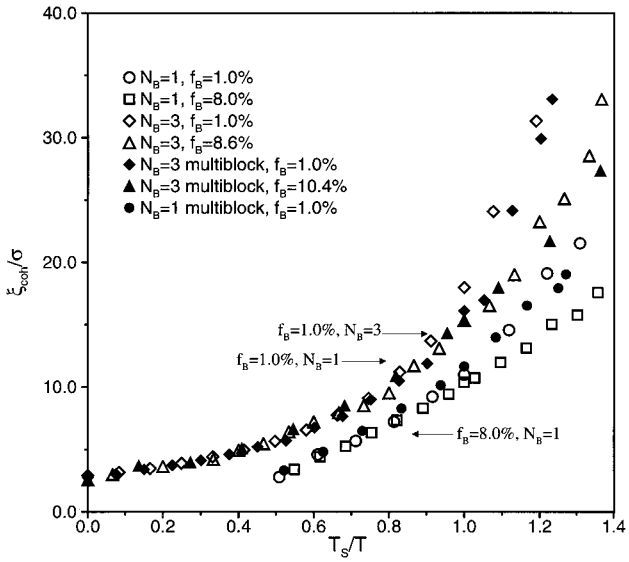

Figure 11. Dimensionless coherence length as a function of reduced inverse temperature for a variety of architectures and B group fractions. Arrows indicate the microdomain period, $D = 2\pi/k^*$, for the telechelic architectures at their spinodal temperatures.

weaker than $1/R_{EE} \propto N^{-0.5}$. Moreover, the near scaling of $k^* \propto N^{-d}$, where d is the dimension of space, is consistent with a morphology of small spherical microdomains of *constant size* embedded in a isotropic dense fluid. If the number of sticky groups in a local cluster increases with f_B, then an even *weaker* dependence of k^* on N is expected. Figure 10 also shows results at fixed absolute (not reduced) temperature corresponding to T_{ODT} of the 8% telechelic. Deviation from simple power law behavior in the direction of smaller microdomain periods, and hence a smaller effective scaling exponent, are found for the low associating group concentration melts since these are well above their respective apparent spinodal temperatures.

The incompressible RPA expression for $\hat{S}_{BB}(k)$ predicts a k^* which is larger (smaller microdomain period) than the PRISM theory result, is *independent* of temperature, and scales as $k^* \propto f_B^{0.05}$. The latter two predictions are in complete disagreement with PRISM theory and experiments on $N_B = 1$ telechelic melts. This failure of the RPA is perhaps not surprising since molecular scale excluded volume interactions are only very crudely taken into account via a long wavelength ($k = 0$) global incompressibility constraint, and an explicit coupling of the attractive BB interactions and packing is not accounted for. Such simplifications are not adequate to describe the structure of very small B group clusters or multiplets.

Figure 11 presents representative results for the microdomain coherence length defined above. Interestingly, at fixed reduced temperature $T/T_s > 1$, a data collapse or scaling behavior applies since the coherence length is virtually independent of associating group concentration and chain architecture for fixed block length N_B. In all cases, at fixed *reduced* temperature the degree of intermultiplet order, as measured by the ratio ξ_{coh}/D, increases monotonically with associating group concentration (or equivalently smaller microdomain period). For example, this trend is reflected in the fact that for the $N_B = 1$ telechelic cases, the coherence length first exceeds the microdomain period at $T_s/T \cong 0.75(1.0)$ for $f_B = 8\%(1\%)$; this temperature could thus be identified with the emergence of strong liquidlike spatial correlations between neighboring multiplets. Upon further cooling to $T \cong T_{ODT}$, the coherence length strongly increases to values $\cong 3(2)D$ for $f_B = 8\%(1\%)$, indicating the emergence of "long-range" correlated liquid order. There is no indication that this growth of the coherence length will stop upon further cooling, although failure of the numerical algorithm[37] at very low temperatures prevents definitive statements. A roughly quadratic dependence of ξ_{coh} on reduced inverse temperature is found.

For comparison, we note that the coherence length $\xi_{coh} \equiv 2\pi/\Delta k_{1/2}$ from the *wide-angle* scattering profile of polyethylene at $T = 430$ K corresponds to $\xi_{coh}/D \approx 2$, where $D = 2\pi/k^*$ and k^* is the location of the amorphous halo peak.[41] Thus, the degree of "short-range order" predicted by our theory for telechelic multiplets at $T = T_{ODT}$ ($\xi_{coh}/D \approx 2-3$)is comparable to that present on a monomer scale in a cold homopolymer melt. For dense atomic fluids modeled as Lennard−Jones spheres,[42] $\xi_{coh}/D = k^*/\Delta k_{1/2} = 2.8(4.6)$ for $\rho^* \equiv \rho\sigma_{LJ}^3 = 0.75(0.844)$ and $T^* \equiv k_B T/\epsilon_{LJ} = 0.83(0.723)$.

C. Majority Phase and Interference Scattering. Experimental measurement of all the partial structure factors is generally not possible. However, the theory provides very detailed information which can contribute to a deeper understanding of the self-assembly process. The majority component *wide-angle* scattering intensity, $\hat{S}_{AA}(k)$, is almost completely independent of temperature for the $N_B = 1$ telechelics, and a discernible low-angle microphase peak does *not* grow in even at T_{ODT}. Physically, this occurs since the structural organization of A monomers is nearly unaffected by physical clustering of the minority B end groups into small clusters.

The cross correlations, $\hat{S}_{AB}(k)$, show several interesting features at low temperatures. Examples in the low-angle region at T_{ODT} are shown in Figure 12. For a $N_B = 1$ and $f_B = 1\%$ ($N = 200$) telechelic, $\hat{S}_{AB}(k) < 0$ in

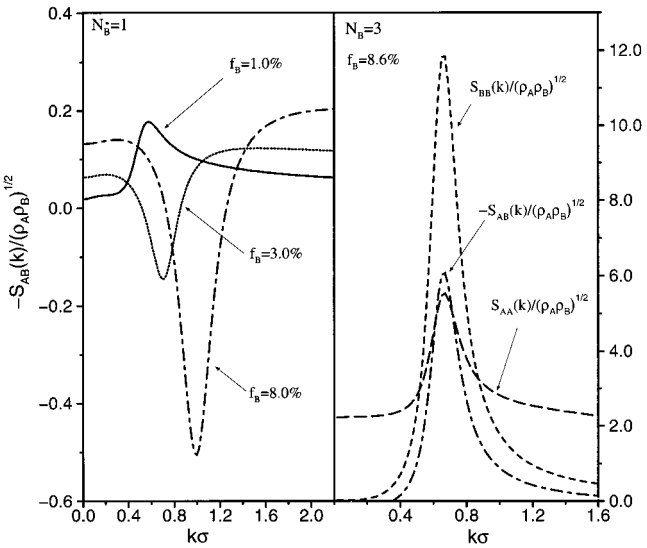

Figure 12. Left panel: Dimensionless AB interference scattering function for several $N_B = 1$ telechelics at their apparent ODT temperature. Right panel: The three dimensionless structure factors for a $N_B = 3$, $f_B = 8.6\%$ telechelic at the ODT.

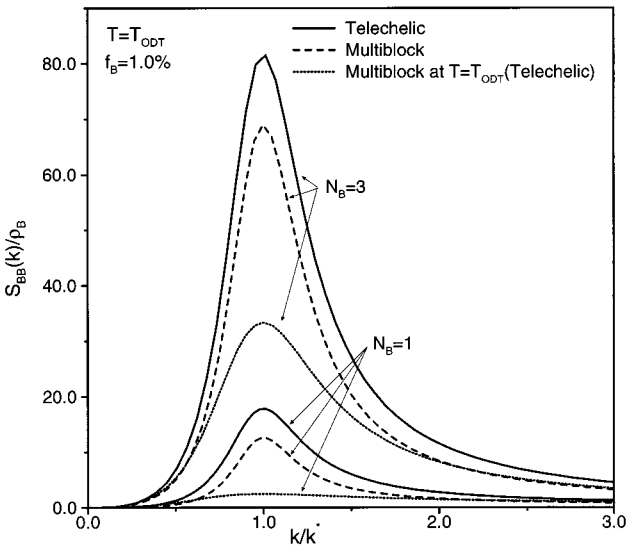

Figure 13. Low wave vector BB dimensionless scattering profiles for several telechelic and multiblock melts as a function of scaled wave vector. Results are shown at the $T = T_{ODT}$ of each system, and a comparison of multiblocks and telechelics is made at a temperature corresponding to the apparent ODT of the telechelic, which emphasizes the much weaker microphase separation of the multiblock architectures at fixed sticky group concentration.

qualitative accord with incompressible RPA-based expectations. But, for higher f_B (smaller N), $\hat{S}_{AB}(k)$ *changes sign* and becomes positive near k^*. Physically, the cross structure factor is probing the correlation of species monomer density fluctuations $\langle \delta\rho_A(r)\delta\rho_B(r')\rangle$ separated in space by a distance $|r - r'| \cong 2\pi/k$. A positive value implies that an excess in A monomer is spatially correlated with an excess in B monomers. Because a significant fraction of A sites on a small telechelic chain are close to B sites, when the B sites self-assemble into clusters, many A monomers are "pulled along" due to chain connectivity, resulting in the sign change of $\hat{S}_{AB}(k)$ for $k \cong k^*$ length scales and the enhancement (relative to the average) of the number of close AB contacts. This effect disappears for the longer $N_B = 1$ telechelics ($f_B = 1\%$), or if the associating group block size increases as shown in Figure 12 for $N_B = 3$. Nevertheless, even for such cases the small wave vector incompressible RPA relations $\hat{S}_{AA}(k) = \hat{S}_{BB}(k) = -\hat{S}_{AB}(k)$ remain very poor.

D. Effect of Block Size and Surfactant Architecture. Examples of the effect of increasing the associating group block size from $N_B = 1$ to 3 have been shown throughout this section in Figures 4, 5, 11, and 12. At fixed f_B, the effect of increasing B group block size (and hence overall degree of polymerization) enhances the B cluster size and microdomain period, which in turn is expected to (a) increase the driving force for microphase separation (at fixed bare driving force $\beta\epsilon_{BB}$), (b) reduce the degree of fluctuation stabilization (nonlinear curvature in the inverse peak intensity vs inverse temperature plot) or equivalently the ratio T_s/T_{ODT}, and (c) enhance the applicability of the incompressible RPA (although it is still quantitatively poor). Trend b is seen in Figure 4; trend a is evident in Figure 5. Trend c is dramatically verified in Figure 12 and calculations of $\hat{S}_{AA}(k^*)$ (see inset of Figure 4), which show a *qualitatively different* T dependence than for the $N_B = 1$ telechelic and the emergence at low temperatures of a low-angle peak in the majority component scattering function.

In terms of the detailed behavior of $\hat{S}_{BB}(k)$ relative to the $N_B = 1$ telechelics, there are some similarities and several distinctive differences, with a few examples shown in Figure 13. We refrain from presenting many plots, and provide only summarizing statements of our findings. (i) In contrast to the $N_B = 1$ cases, for $N_B = 3$ telechelics there does emerge the standard (but weak) low-angle "correlation hole" peak under athermal conditions, and as expected, the incompressible RPA relations and shape of the scattering function are in better (but still not good) agreement with compressible PRISM theory. (ii) At low temperatures the scattering profile is narrower. (iii) The wide-angle peak behavior is essentially the same. (iv) Consistent with Figure 11, in the low-temperature regime, the T-dependencies of $\hat{S}_{BB}(k^*)$ and ξ_{coh} are stronger. (v) k^* is quantitatively smaller for obvious reasons of a larger N_B, but again saturates at low T, and follows the same $k^* \propto f_B^{0.31} \propto N^{-0.31}$ law found for the $N_B = 1$ telechelics. Interestingly, for this larger B cluster case the incompressible RPA prediction, $k^* \propto f_B^{0.26}$, is now reasonable. (vi) The same $T_s \propto f_B^{0.8}$ law is found. (vii) Porod plots at T_s and T_{ODT} look very similar to the $N_B = 1$ cases in Figure 9.

The surfactant, or "monotelechelic", architecture (see Figure 1) has also been examined and contrasted with its telechelic analogues. The case of $N_B = 1$, $f_B = 0.5-5\%$ (corresponding to $N = 20-200$) was examined at the same reduced packing fraction as for the analogous telechelics. We find that, (i) at constant associating group fraction f_B, the quantities $\hat{S}_{BB}(k)$, T_s, and T_{ODT} are nearly identical (to within less than 5%) to their telechelic analogues and (ii) all apparent scaling relations discussed for telechelics are same for the corresponding surfactants. This lack of sensitivity of the equilibrium microphase segregation phenomena to whether the chain has sticky groups at one or both ends is perhaps not surprising, especially since the two ends of telechelics do not reside in nearest neighbor microdomains and thus will not "interfere" much with each other. Of course, the dynamic and mechanical properties of surfactants and telechelics are in general very different since only telechelics form thermoreversible

networks, while surfactants self-assemble into "starlike" entities.[1]

Finally, we briefly summarize our findings for the influence of closure approximation on the results described in this section; a more detailed discussion is given in Appendix C. As expected, the temperature dependence of the BB scattering profile features such as inverse peak intensity (Figure 4), microdomain period (Figure 10), and coherence length (Figure 11) are significantly changed if the nonlinear RMPY/HTA closure of eq 2.17 is employed. The onset of strong clustering is more abrupt resulting in a sigmoidal shape for the $\hat{S}_{BB}^{-1}(k^*)$ vs T^{-1} plot and the detailed form of the temperature dependencies of k^* and ξ_{coh}. Thus, the apparent (extrapolated) spinodal temperature occurs at a significantly higher value and is in fact in better agreement with the crude a priori estimates of ϵ_{BB} described in section IIA. On the other hand, the low-temperature nonlinear fluctuation stabilization regime remain similar to that shown in Figure 4, and relative features such as the dependence of T_s on associating group concentration, B block length, and architecture remain qualitatively similar. Moreover, the predictions of the two closures for structural properties are often quantitatively similar (nearly identical) when compared at fixed reduced temperature T/T_s (fixed peak intensity or order parameter amplitude $\hat{S}_{BB}(k^*)$).

IV. Multiblocks

The consequences of changing from relatively short end-associating polymers to a long chain regular multiblock architecture has been investigated. Intuitively, one expects that such larger N multiblocks will exhibit reduced tendency to form clusters at fixed bare driving force ($\beta\epsilon_{BB}$) since the sticky monomers are bonded to neutral A groups on both sides and will experience more entropically driven "shielding" from the (now longer) polymer coil. Thus, chain connectivity, larger degree of polymerization, and excluded volume constraints will all act in concert to reduce the ability of B sites in multiblocks to form tight multiplets. Hence, we expect a lowering of T_s and T_{ODT} and weaker signatures of microphase separation in $\hat{S}_{BB}(k)$. On the other hand, for these same physical reasons, one expects that the clustering of sticky B monomers will have a larger perturbation on the structure of the majority A component, and this might be revealed as temperature-induced modifications of the low-angle region of $\hat{S}_{AA}(k)$.

All the above qualitative expectations are borne out by our calculations. We explicitly present only a few representative results to make these points. Consider first the $N_B = 3$ block size; we have studied chains of $N = 1000$ and $f_B = 1$, 2.4, 4.8, 5.4, and 10.4%, at an overall packing fraction of $\eta = 0.4$ chosen to yield a dimensionless compressibility very close to that characteristic of the shorter chain telechelic systems ($\hat{S}(0) \cong 0.25$) studied in section III. A few results for $N_B = 5$ and $N_B = 1$ have also been obtained. The former case begins approaching the more classic multiblock copolymer system; however, there are still strong deviations from the $\hat{S}_{AA}(k) = \hat{S}_{BB}(k) = -\hat{S}_{AB}(k)$ incompressible RPA type relation. Moreover, the shape of $\hat{S}_{AA}^{-1}(k^*)$ vs T^{-1} is strongly sigmoidal, a feature apparently seen experimentally in multiblock polyurethane copolymer melts.[43] The $N_B = 1$ case was particularly hard to obtain converged numerical solutions for, and we only report results for $f_B = 1\%$. We note that for $N_B = 1$ *random* multiblock ionomers, there will be regions along the chain where $N_B > 1$ locally; thus, our $N_B > 1$ regular multiblock calculations may have some relevance for such systems also.

Figure 4 contains one example of how the fluctuation stabilization process is (weakly) enhanced by going to the multiblock architecture relative to the analogous telechelic (although relative trends with N_B and f_B remain the same). The enhanced fluctuation stabilization is primarily a reflection of the reduced microdomain period of multiblocks relative to telechelics at fixed reduced temperature and f_B (see inset of Figure 10). The latter effect enhances the coupling between microdomain scale fluctuations and local packing, which is the physical origin of the enthalpically driven fluctuation stabilization process within PRISM theory.[19]

Figure 5 demonstrates the *large qualitative* changes in the dependence of the apparent spinodal temperature on associating group concentration for multiblocks. For the $N_B = 3$ and 5 cases, *much weaker* (relative to the telechelics) empirical power laws, $T_s \propto f_B^{0.48}$ and $f_B^{0.41}$, are found, which are also very different than the corresponding RPA multiblock predictions of $T_s \propto f_B^{0.8}$ and $f_B^{0.7}$. Moreover, the absolute value of the apparent spinodal temperature is even smaller relative to the RPA values, more so as the fraction of sticky groups increases. These differences between telechelics and multiblocks reflect the more crowded environment of A groups in the vicinity of the sticky B groups distributed uniformly along the polymer backbone which sterically frustrates, in a f_B-dependent fashion, B-group self-assembly within PRISM theory (but which is *not* accounted for on the basis of the RPA). At constant absolute T, this feature leads to much broader and less intense structure factors $\hat{S}_{BB}(k)$ for the multiblock polymers compared to their telechelic analogues, which becomes even more dramatic with increasing associating group concentration. An example of this behavior is shown in Figure 13**.** All these trends are consistent with physical arguments presented in the beginning of this section.

At constant *reduced* temperature, very similar $\hat{S}_{BB}(k)$ are found, although the multiblock scattering profiles are still quantitatively broader and slightly less intense. Examples of this trend are also shown in Figure 13 for $f_B = 1\%$ and $N_B = 1$ and 3 cases. Note also that increasing the sticky block length results in a much larger enhancement of the microdomain scattering intensity and hence physical clustering for multiblock copolymers compared to the analogous telechelic.

Some details of the T dependence of $\hat{S}_{BB}(k)$ for multiblocks $N_B = 3$ are contained in Figure 11, and others can be briefly summarized as follows. (a) At fixed f_B and *reduced* temperature, the coherence length for multiblocks and telechelics is quite similar in absolute magnitude, as is their (low) temperature dependence of the ratio ξ_{coh}/D. (b) As found for the $N_B = 1$ telechelics, the temperature dependence of the order parameter (not plotted) can be well fit by an exponential, $\hat{S}_{BB}(k^*) \propto e^{c\beta\epsilon_{BB}f_B^{\nu}}$, where c is a numerical constant and $\nu \cong 0.34(0.25)$ for $N_B = 3(5)$. However, for the telechelics, a significantly larger exponent of $\nu \cong {}^2/_3$, was found, consistent with the much stronger dependence of T_s on f_B displayed by telechelics. (c) k^* is quantitatively larger (smaller domain size) than telechelics at fixed f_B, again suggestive of weaker clustering. An example is shown in the inset of Figure 10. At low T, k^* again saturates,

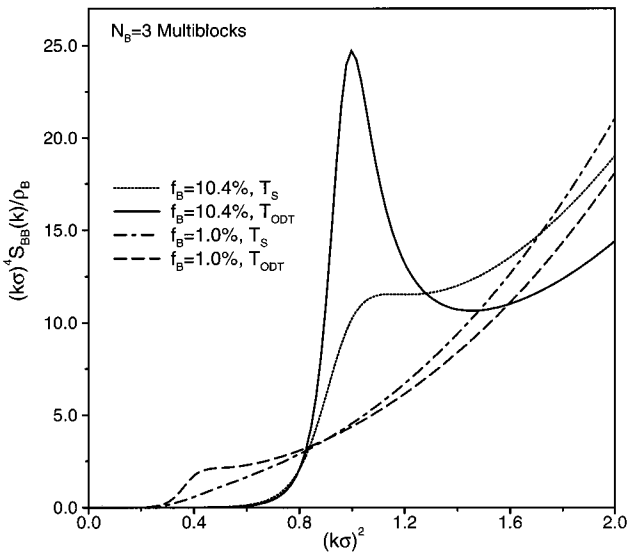

Figure 14. Porod plot for $N_B = 3$ multiblocks for two values of f_B at the apparent spinodal temperature and ODT.

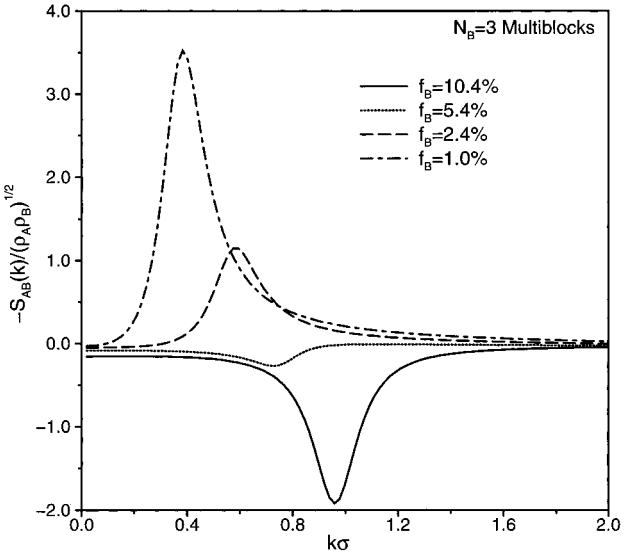

Figure 15. Interference AB structure factor for $N_B = 3$ multiblocks and various values of B group concentration.

and follows the law $k^* \propto f_B^{0.37}$, slightly stronger than the $f_B^{0.31}$ law found for telechelics. This latter trend follows from the elementary fact the mean squared end-to-end distance between neighboring B blocks along the chain is numerically found to obey the apparent scaling law $R_{EE,block} \propto N^{0.55}$ in contrast to the $N^{0.5}$ law for the telechelic overall chain end-to-end distance. Since the microdomain period is again smaller than the end-to-end distance separating the middle of two nearest neighbor sticky groups (or blocks) along the chain ($R_{EE,block} > D$), the same real space physical picture as described for the telechelics applies. For both the $N_B = 3$ and 5 cases, at the apparent ODT we find $R_{EE,block}/D = 1.10$, 1.25, and 1.74 for $f_B = 10.3\%$, 4.8%, and 0.9% respectively. For a $N_B = 1$, $f_B = 1\%$ multiblock, $R_{EE,block}/D = 1.43$ at the apparent ODT, considerably smaller than its longer block counterparts. (d) The Porod plots in Figure 14 show somewhat more structure than for the analogous telechelics in Figure 9, but very small interfacial widths on the order of an angstrom are still found at low temperatures.

As shown in Figure 15 the cross correlation structure factor for the $N_B = 3$ multiblocks displays a strong non-RPA behavior, including the sign changes for the 10.4% multiblock similar to what was seen for $N_B = 1$ telechelics (see Figure 12), presumably for the same physical reasons discussed in section IIIB. However, it is interesting to note that the analogous $N_B = 3$ telechelics do *not* show the sign changes, suggesting that perturbation of the A domain packing is much more significant for the multiblock architecture than for the end-labeled telechelics. For the larger $N_B = 5$ multiblock cases (not shown), no sign changes are observed, and the standard low-angle $\hat{S}_{AB}(k) < 0$ incompressible RPA prediction holds.

Finally, as expected, the wide-angle scattering (not shown) associated with monomer scale order behaves in essentially the same weakly varying manner as found for the telechelics.

V. Comparison with Experiments

The theoretical results reveal many systematic trends in small-angle scattering profiles and microdomain scale structure as a function of temperature, attractive interaction strength ϵ_{BB}, associating group concentration f_B, sticky group block size N_B, and global architecture. In principle, these predicted trends can be compared with experiments. Unfortunately, there are rather few detailed quantitative studies of ionomer melts which address our predictions. One source of difficulty is the common use of high T_g polystyrene ionomers, which makes equilibrium thermal melt studies very difficult.[1] The presence of excess low-angle scattering ("$k = 0$ upturn"), absent in our equilibrium statistical mechanical theory, is believed to arise from a weak but long-range *non*equilibrium distribution of ionic groups and can interfere with quantitative analysis of the microdomain scattering peak.[1,5] The apparent lack of any true observable phase transition temperature in most experiments makes it effectively impossible to directly analyze data in our language of a reduced temperature, T/T_s or T/T_{ODT}. Nevertheless, in this section, we summarize experimental scattering studies and compare them semiquantitatively with theoretical scattering profile results.

A. Telechelics. Most experiments have concerned carboxylated or sulfonated polyisoprene (c-PI, s-PI) or the polybutadiene (PBD) analogue for the standard $N_B = 1$ case. Williams et al.[3] studied a c-PBD telechelic of $N \cong 85$ ($f_B \cong 2.4\%$) with a variety of metal cations. At room temperature, the SAXS peak was found in the range $k^* \cong 0.083-0.12$ Å^{-1} depending on the metal cation. We compare this with our theoretical result for a 2% ($N_B = 1$) telechelic at T_{ODT} of $k^* = 0.743\sigma^{-1}$. If one identifies a single spherical site of the semiflexible chain (of aspect ratio $\Gamma = {}^4/_3$) as a PBD monomer, then on the basis of the known molar volume of PBD of ≅65 Å^3, the effective $\sigma \cong 5$ Å, yielding $k^* \cong 0.15$ Å^{-1}. The agreement is only rough, but this is perhaps to be expected due to our crude model of PBD chain structure and assumption that a single "bead" is equivalent to one real monomer. Small re-interpretations of the correspondence between real monomers and our tangent beads and/or adjustment of the model chain persistence length to better mimic the $\Gamma \cong 1$ value appropriate for PBD can easily account for the difference. The theoretical value of $\beta_{ODT}\epsilon_{BB} \cong 20$ for a 2% telechelic (see Figure 5) may be a bit high, but it would seem to lie at the upper end of an experimentally realizable range.[1]

Williams et al.[3] also studied the above c-PBD telechelic melt over a wide temperature range of 25−209 °C, corresponding to change of our theoretical parameter $\beta\epsilon_{BB}$ by a factor of ≅1.6. Over this temperature range, the small-angle scattering profile decreased dramatically in peak intensity and broadened significantly (by a factor of ≅3), and k^* increased by ≅35%. At room temperature, a measure of the ratio of the microdomain period to coherence length scale, $\Delta k_{1/2}/k^*$, takes on a value of ≅ 0.3−0.4.[44] All these trends and numerical values are in qualitative agreement with our theoretical results (see Figures 6, 10, and 11). The much greater thermal sensitivity of the peak breadth compared to its location is noteworthy. On the basis of the assumption that the experimental temperature regime falls near the theoretical T_s value, there is good semiquantitative agreement. Many workers have found from a Porod analysis a small value for the multiplet size of 6−10 Å and an interface width between the ionic and neutral groups of a few angstroms or less.[1−3] These results are also in agreement with our calculations reported in section IIIB and our following companion paper. Experiments on a series of c-PI telechelics,[3] where N varied from ≅100−500, found a monotonic decrease of k^* with N which could be fit by several functional forms, including a $N^{-1/3}$ law as we found in Figure 10.

Several workers have studied the changes in small-angle scattering of PI telechelics when the acid is changed from carboxylate to sulfonate.[1,2] All find that s-PI displays more order as manifested in smaller values of k^* (larger microdomain length scale by typically a factor of 1.1−1.4) and narrower scattering profiles (smaller values of $\Delta k_{1/2}/k^*$, often by factors of 2−3). These trends are qualitatively consistent with the theory since changing the anion from carboxylate to sulfonate at a fixed temperature increases the effective value $\beta\epsilon_{BB}$, or equivalently lowers the reduce temperature T/T_s.

Experiments by Sobry et al.[2] indicate that increases in chain length (or equivalently reduction of f_B) for several c-PI and s-PI melts ($f_B \cong 1-3\%$) also results in significant broadening of the scattering curve indicative of an effective increase of dimensionless temperature in accord with the theoretical results. For c-PI melts, the ratio of the microdomain period to end-to-end distance is found to be in the range $D/R_{EE} \cong 0.65-0.74$, which is less than unity and a decreasing function of chain length, consistent with our results in section III. However, for the s-PI melt D/R_{EE} is much larger (≅0.9−1.0), and roughly independent of ion content, implying a different $D \propto R_{EE} \propto N^{1/2}$ type scaling. Vanhoorne et al.[45] found a $k^* \propto N^{-1/3}$ law for sulfonated polystyrene concentrated solutions, and changing from a telechelic to surfactant architecture made virtually no difference, in qualitative accord with our theoretical results.

All the above telechelic experiments are significant in the general sense that changes in temperature, acid anion type, and/or sticky group concentration result in changes in the small-angle scattering indicative of significant modifications of the degree of clustering and microdomain scale order. This suggests that the self-assembly process is incomplete in the range of effective $\beta\epsilon_{BB}$ values being probed by most experiments, and a very low temperature "super-strong segregation" type regime may often not be applicable.

Finally, Venkateshwaran et al.[4] have studied a few ionomer melt telechelics with associating blocks of N_B = 2−5 monomers ("mini-triblocks") for $f_B \cong 4-10\%$. Here, scattering from the pure acid forms does display low-angle microphase peaks, and both k^* and profile line widths decreased significantly with increasing sticky block length (with $\Delta k_{1/2}/k^* \cong 0.2-0.4$ typically). The latter trends are understandable as a consequence of large cluster sizes and more complete microphase separation as the sticky block size increases and are in qualitative agreement with the theoretical results presented in section IIID.

B. Multiblocks. The multiblock systems most relevant for comparison with our present theory are regular, or periodic, ionomers, for which there exist little data. Cooper, Register, and co-workers have studied regular sulfonated polyurethane based polyol multiblocks, including one case over the broad range of 22−200 °C in temperature.[7] Upon heating, they find strong evidence of significant reduction of microphase order and clustering, with even a hint of complete dissolution (corresponding to $T \gg T_s$) of ionic groups for a Zn-neutralized material. With increasing temperature (or decreasing ionic group concentration), the low-angle scattering profiles decrease in peak intensity, dramatically increase in breadth, and shift to higher wave vectors by 10−15%. Variable ionic group concentration studies show that the peak wave vector shifts can be described roughly as $N_B^{-1/3}$, where N_B is the number of monomers between neighboring ionic groups. All these trends are in qualitative agreement with our theoretical results of section IV.

Most multiblock experiments involve materials where the ionic groups are distributed at random along the chain. Despite this quenched disorder, almost all the major trends seen in small-angle scattering experiments discussed above remain the same as observed for regular multiblocks and telechelics. Several workers have studied sulfonated polystyrene (s-PS) multiblock melts.[5,6,46] For Na and Zn neutralized s-PS of $f_B \cong 1\%$, values of k^* in the range of 0.13−0.14 Å^{-1} have been reported. Our theoretical results for a 1%, $N_B = 1$ regular multiblock yield a low-temperature value of $k^* \cong 0.725\ \sigma^{-1}$. Again assuming that one "site" of our crude polymer chain model corresponds to one polystyrene monomer, we estimate, based on the known PS molar volume, that $\sigma \cong 6$ Å. This yields a theoretical value of $k^* \cong 0.12$ Å^{-1}, in (perhaps fortuitously) good agreement with the experiment.

We do note that for random multiblocks the characteristic wave vector is much less sensitive to block length N_B, with $k^* \propto N_B^{-1/6}$ reported for several materials,[11] which is *not* in agreement with our theoretical findings for regular multiblocks. This may directly reflect the consequences of quenched randomness on microdomain structure. At a more quantitative level, the multiblock ionomers appear to display broader scattering profiles (typically a $\Delta k_{1/2}/k^*$ roughly twice as large) than their telechelic counterparts at fixed T and f_B, consistent with the expectation of stronger clustering in the latter as found in our theoretical studies. There are few systematic, equilibrium thermal studies since polystyrene-based ionomers are the dominant material examined. However, Weiss and Lefelar[6] and Chu et al.[46] have found evidence for significant reduction in clustering and microdomain order in Zn-based s-PS above 250 °C.

In conclusion, we believe there is reasonable qualitative, and sometimes nearly quantitative, agreement

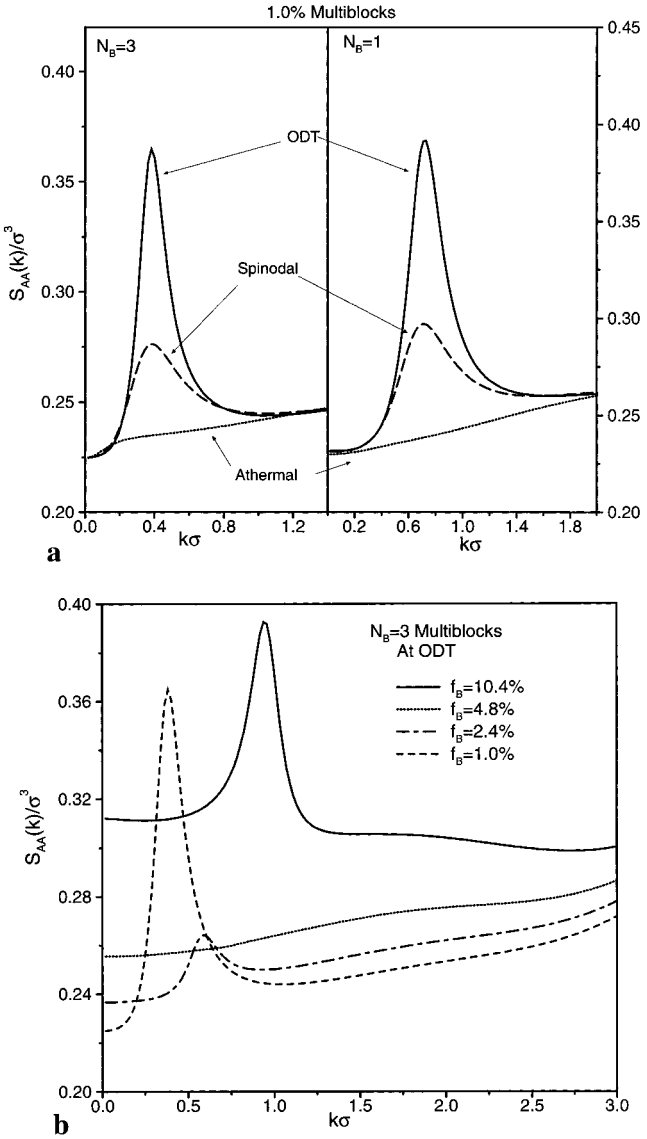

Figure 16. (a) Majority component scattering profile for $N_B = 1$ and 3, $f_B = 1\%$ multiblocks at the three indicated temperatures. Note the absence of any small-angle peak in the athermal limit. (b) Same quantity as in part a but for $N_B = 3$ multiblocks and four sticky group concentrations at the ODT.

between theory and SAXS experiments on the "ionomer peak", especially for telechelic ionomer melts. This provides encouragement for further theoretical analysis of structural properties which are difficult or impossible to experimentally extract. These include the local and intermediate scale interchain packing information and real space correlations presented in the following paper.

C. "Clusters" vs "Multiplets" and Mechanical Properties. The majority component scattering function peak intensity $\hat{S}_{AA}(k^*)$ for multiblocks is found (inset of Figure 4) to have more T dependence than telechelics and begins to take on a sigmoidal shape with increasing N_B and/or f_B. For both the $N_B = 1$ and 3 multiblocks, in the athermal limit there are either no (low f_B case) or very weak small-angle peaks in $\hat{S}_{AA}(k)$. However, when the system is cooled to T_s and below, significant microphase scale peaks grow in. An example for the 1% multiblocks is shown in Figure 16a; very similar behavior is found for the $N_B = 1$ and 3 cases studied. Moreover, the emergence of a small-angle peak in the majority phase scattering for the $N_B = 1$ multiblock has *no counterpart* for the telechelic or surfactant architectures. This is consistent with the idea that multiplet formation perturbs the majority component to a much greater degree for multiblock ionomers compared to their telechelic counterparts. The sticky group concentration dependence of this effect at T_{ODT} is shown in Figure 16b for the $N_B = 3$ multiblock case (which we expect based in Figure 16a to be qualitatively the same as would be found for the $N_B = 1$ multiblocks). Significant microdomain scale peaks emerge for the lowest and highest sticky group concentrations. However, at intermediate values of $f_B = 2.4$ and 4.8%, much weaker or nonexistent peaks are found.

The intriguing nonmonotonic dependence of $\hat{S}_{AA}(k)$ on multiblock B group concentration is suggestive of the presence of two distinct physical processes acting in opposite directions. Figure 15 shows the analogous results for the cross correlation function $\hat{S}_{AB}(k)$. For $f_B = 1\%$, $\hat{S}_{AB}(k) < 0$ in accord with an incompressible RPA picture of segregation: in a chain-averaged sense, the density of majority A groups in the vicinity of the small B clusters are *less* than their bulk value (yielding a $\delta\rho_A(r) = \rho_A(r) - \rho_A < 0$), thereby resulting in a *negative* low-angle peak in $\hat{S}_{AB}(k)$ for the standard "correlation hole" reason for large scale incompressibility and chain connectivity. However, with increasing sticky group concentration, and hence decreasing microdomain period, the AB scattering amplitude decreases and eventually *changes sign* for the 10.4% multiblock indicative of the correlated *densification* of A groups near the small B clusters. At intermediate sticky group concentrations, we suggest there is a near cancellation of these two effects, resulting in the features seen in Figure 16b. Thus, the presence of positive amplitude small-angle peaks in the majority component scattering is suggested to arise for *entirely different* physical reasons in the 1% and 10.4% multiblock cases. Moreover, our results suggest that an ionic group threshold needs to be exceeded for the emergence of a material where A groups are densified in a correlated manner in the vicinity of the B group multiplets and that such a phenomenon does *not* occur for the $N_B = 1$ telechelic or surfactant architectures.

Eisenberg et al.[16] have proposed a "restricted mobility" model which proposes that there exists a small region around the B group multiplets of diminished A monomer mobility. At high enough ionic group concentration, such regions may overlap and form continuous "clusters". Invoking dynamic percolation type ideas, one then concludes that the material will exhibit two distinctly dynamic responses, resulting in the observation of two glass transitions or peaks in mechanical loss spectra. We speculate that our observation of A group reorganization on the microdomain scale for $N_B = 1$ multiblocks of sufficiently high sticky group concentration may possibly be a fundamental structural feature underlying the "dynamic cluster" transition in ionomer melts. Following this logic, similar effects may occur in telechelics, but our theoretical results suggest that *higher* degrees of ionic group concentration than required for multiblocks and/or *blocky* telechelics (e.g., the $N_B = 3$) are needed to observe similar dynamic mechanical consequences. Neutron-scattering experiments where the *majority block* was selectively deuterated might allow direct testing of our predictions for $\hat{S}_{AA}(k)$ in the low-angle region.

VI. Summary and Discussion

We have presented the first microscopic liquid state theory of the structure of strongly associating heteropolymers melts. This paper has focused on the consequences of multiplet and microdomain formation on partial small-angle scattering profiles. The self-assembly process as probed by such collective scattering functions has been found to depend in a rich manner on the experimental control parameters such as temperature, chemical interaction strength ϵ_{BB}, associating group concentration f_B, sticky group block size N_B, and global architecture (telechelic, regular multiblock, surfactant). End-functionalized telechelic and surfactant architectures are found to behave nearly identically and to form more (short range) ordered microphase structures at higher temperatures than their (periodic) multiblock counterparts. There are significant differences between telechelics composed of unimer sticky groups ($N_B = 1$) vs the $N_B = 3$ "mini-triblocks". The latter behave much more like classic block copolymers, although strong deviations from simple incompressible RPA predictions are still found for $N_B = 3$ and 5. Qualitative comparison with experimental SAXS studies of ionomers reveals significant qualitative, and sometimes semiquantitative, agreement. However, more systematic and quantitative SAXS studies, especially of model telechelic materials over a wide range of temperature, are required to further test our results. The theory also provides the majority component and AB interference partial structure factors which provide additional insight into the self-assembly process. For these quantities, distinctive differences emerge between $N_B = 1$ and 3 telechelics, telechelics and multiblocks, and various f_B cases within a given architecture. Experimental testing of our results using deuteron-labeled materials and neutron scattering would be very interesting.

It would be highly desirable to test our theoretical results against many chain computer simulations of dense melts. Unfortunately, this is a very demanding computational problem, and the only study we are aware of focuses on a 2-dimensional lattice model for a single value of $\beta\epsilon_{BB} = 3$ or, most recently, very short 3-dimensional continuum chains.[25] This work does not allow meaningful conclusions to be drawn regarding the accuracy of our present theory. Prior theories for the small-angle scattering function are phenomenological in nature. The modified hard sphere "liquidlike-order" model of Cooper and co-workers[18] is closest in spirit to what our microscopic theory has found, and a detailed comparison with this approach is given in the following paper.

We would like to emphasize that the availability of a microscopic theory of the structure (on all length scales) of associating polymer melts will provide useful input into molecular level descriptions of other interesting phenomena which are strongly influenced by clustering and microdomain formation. These include collective stress relaxation, single chain dynamics of unentangled and entangled melts,[47] thermoreversible gelation and network formation, and perhaps modification of the glass transition due to sticky group microphase separation.

Finally, the present work represents only the first step toward a more complete and accurate microscopic theory. The role of closure approximation for structured fluids which interact via strong attractive forces requires further study. The detailed temperature dependencies predicted by the theory are expected to be sensitive to the specific statistical mechanical approximation adopted, although the limiting high and low temperature predictions and the qualitative influence of temperature should be insensitive. Benchmark computer simulations would be very valuable for testing and designing improved closures. The chain model employed in this paper neglected many angstrom level chemical details. This simplification is easily relaxed within the PRISM formalism at the expense of additional numerical effort and more interaction potential parameters.[29] For simplicity, we also assumed that the clustering process does not perturb polymer conformation. Under some circumstances, this is potentially a serious oversimplification, which can be avoided by employing more advanced "self-consistent" versions of the PRISM approach.[29] For dense ionomer melts, experiments suggest conformational perturbations are indeed weak,[1,34] although this will surely break down in solution. The theory has been generalized to treat ionomer solutions and blends, including an explicit representation of solvent molecules and whether they act as neutral plasticizers or highly selective additives.[48] This generalization opens the possibility to study the influence of solvent dilution on multiplet formation and also competition between macrophase separation and microdomain ordering. Explicit accounting for the quenched chemical disorder present in random ionomers is a larger challenge for polymer integral equation theory, which at present remains unsolved.

Acknowledgment. This work was supported by the U.S. Department of Energy, Division of Materials Science, Grant DEFG02-96ER45439, through the University of Illinois at Urbana—Champaign, Frederick Seitz Materials Research Laboratory. Helpful discussions and/or correspondence with Professors Ben Chu, Rick Register, and Robert Weiss are gratefully acknowledged.

Appendix A: Intramolecular Distribution Functions

Numerical calculation of single chain site−site distribution functions, $\hat{\omega}_{\alpha M,\gamma M'}(k)$, for the semiflexible chain model which are required to compute $\hat{\omega}_{MM'}(k)$ in eqs 2.3−2.12 have been discussed in great depth previously.[32] Their general form is

$$\hat{\omega}_{\alpha M,\gamma M'}(k) = \frac{\sin(B_M k)}{B_M k}\, e^{-A_M{}^2 k^2} \qquad \text{(A.1)}$$

where

$$A_M{}^2 = \frac{1}{6}(1 - C_M)\langle r_{\alpha M,\gamma M'}{}^2\rangle, \quad B_M{}^2 = C_M\langle r_{\alpha M,\gamma M}{}^2\rangle,$$
$$\text{and } C_M{}^2 = \frac{1}{2}\left(5 - 3\,\frac{\langle r_{\alpha M,\gamma M'}{}^4\rangle}{\langle r_{\alpha M,\gamma M'}{}^2\rangle^2}\right) \qquad \text{(A.2)}$$

Explicit expressions for the second and fourth moments are quite lengthy, and are given elsewhere.[32]

Appendix B: RPA and Thread PRISM Models

If the hard core diameter of polymer sites goes to zero, $\sigma \to 0$, then one obtains the so-called "thread" model used extensively in analytic PRISM studies.[29] In this "toy model" limit, the convolutions in the molecular closure expressions of eq 2.13 can be canceled, and

deterministic expressions for the direct correlation functions are obtained. The linearized RMPY/HTA of eq 2.18 yields[29]

$$\hat{C}_{AA}(k) = \hat{C}_{AB}(k) = \hat{C}^{(0)}(k),$$
$$\text{and } \hat{C}_{BB}(k) = C^{(0)}(k) + \beta|V_{BB}| \quad \text{(B.1)}$$

where $|V_{BB}| = \int d\vec{r} V_{BB}(r)$ and $g^{(0)}_{BB}(r)$ has been set to unity to facilitate comparison with Flory−Huggins-type RPA approaches (see below). In the naive thread limit, the effect of repulsive and attractive forces enter the effective potentials independently, in the spirit of the classic RPA. On the basis of such a thread limit, PRISM theory does predict a true spinodal phase transition corresponding to $\hat{S}_{MM'}(k^*) \to \infty$. Substituting eq B.1 into eq 2.11 yields the spinodal temperature, or equivalently the value of the bare χ-parameter corresponding to the spinodal condition, $\chi_{0,s}$:

$$\frac{k_B T_s}{|V_{BB}|} = \frac{\rho_m(f_B\hat{\omega}_{BB} - f_A f_B \delta\hat{\omega}(\rho_m\hat{C}^{(0)}))}{1 - \rho_m\hat{C}^{(0)}(f_A\hat{\omega}_{AA} + f_B\hat{\omega}_{BB} + 2\omega_{AB})} \propto \chi_{0,s}^{-1} \quad \text{(B.2)}$$

where all the wave vector dependent functions are evaluated at $k = k^*$, defined implicitly by the condition that T_s is a maximum at k^*.

As is well-known,[29] the incompressible RPA limit can then be obtained by allowing $-\hat{C}^{(0)}(k^*) \to \infty$, thereby yielding the RPA spinodal condition, $2\chi_0 = F \propto T_s^{-1}$ where

$$F = \frac{1}{\delta\hat{\omega}}\left(\frac{\hat{\omega}_{AA}}{f_B} + \frac{\hat{\omega}_{BB}}{f_A} + \frac{2\hat{\omega}_{AB}}{f_A f_B}\right) \quad \text{(B.3)}$$

and the RPA scattering function $\hat{S}(k) = (F - 2\chi_0)^{-1} = \hat{S}_{AA}(k) = \hat{S}_{BB}(k) = -S_{AB}(k)$. In the main text, we discuss the predictions for T_s of these simplified approaches using the same numerical Koyama models for the intrachain correlation functions employed in the full PRISM studies. For the high meltlike conditions of present interest, eqs B.2 and B.3 yield nearly identical results in the sense that all qualitative trends for T_s as a function of associating group concentration, block size, and overall chain architecture are virtually identical. Thus, in the main body of the text, we discuss only the incompressible RPA predictions.

For nonzero thickness chains, the thread PRISM and RPA approaches do not properly enforce the hard core exclusion constraint that $g_{MM'}(r) = 0$ for $r < \sigma$ under thermal conditions. Thus, differences between the RPA and full numerical PRISM predictions for the magnitude and qualitative trends of T_s as a function of associating polymer structure arise from the modification of the consequences of the strong BB attractions due to steric constraints captured by enforcing the local hard core impenetrability constraint and chain connectivity.

Appendix C: Alternative Closures and Potential Models

It is of interest to study the nonlinear version of the RMPY/HTA molecular closure, eq 2.17, and contrast PRISM predictions based on it with the linear analogue used in the main body of the text, eq 2.18. In this Appendix, we summarize our limited numerical studies of this alternative nonlinear closure, and present a few representative plots.

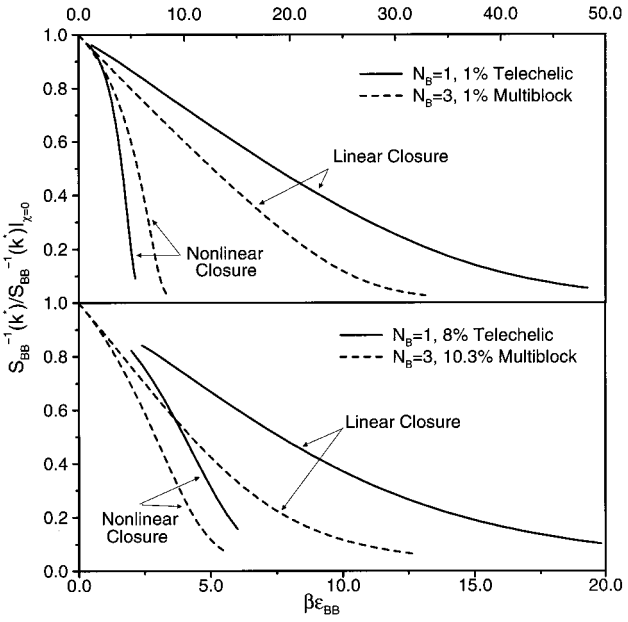

Figure 17. Inverse BB peak scattering intensity normalized by its athermal value as a function of reduced temperature for two $N_B = 1$ telechelics and two $N_B = 3$ multiblock melts. Predictions of the linearized and nonlinear RMPY/HTA closure approximations are compared.

We have first studied $N_B = 1$ telechelics with $f_B = 1$, 3, and 8%. Examples of the $\hat{S}_{BB}(k^*)$ peak intensity cooling curves are shown in Figure 17. As required, agreement between the two closures is found at high temperatures where $\beta\epsilon_{BB}$ is small, but increasing differences are observed as the fluid gets colder. Strong concentration fluctuations and clustering occur at much higher temperatures based on the nonlinear closure, in a manner which becomes more pronounced with decreasing associating group concentration f_B, The numerical Picard iteration algorithm fails to converge[37] when the peak scattering intensity reaches a rather large value, which is nearly the same for both closures and different models. For the nonlinear closure this corresponds to $\beta\epsilon_{BB} = 3.4$, 4.5, and 5.6 for $f_B = 1$, 3 and 8%. Such values can be taken as very crude estimates of a spinodal temperature, T_s. They range from factors of $\cong$3 ($f_B = 8\%$) to $\cong$8.6 ($f_B = 1\%$) larger than found for the (extrapolated) spinodals based on the linearized RMPY/HTA closure results and correspond to values of the BB attraction energy in rough agreement with crude a priori estimates for ionomers discussed in section II.

Roughly speaking, the mathematical structure of the two closures in eqs 2.17 and 2.18 suggest that $\beta\epsilon_{BB}$ of the nonlinear closure will approximately correspond to $\ln\{1 + \beta\epsilon_{BB}\}$ of the linearized closure; that is, for very strong BB attractions the strength of the effective interaction between associating groups will grow exponentially with $\beta\epsilon_{BB}$ based on the nonlinear closure, as might be intuitively expected. Note also that the initial stages of a low-temperature fluctuation stabilization regime can be detected in the nonlinear closure results as must occur since no true spinodal divergences can occur.[19]

The actual shapes of $\hat{S}_{BB}(k)$ based on the two closures are very similar (not shown), but their temperature dependencies are significantly different in the low-temperature regime. An empirical mapping of the

temperature scales of the two closure results based on the $[\beta\epsilon_{BB}]_{NONLINEAR} \leftrightarrow \ln\{1 + \beta\epsilon_{BB}\}_{LINEAR}$ connection suggested above provides a partial collapse of structure factor predictions but is far from perfect. However, relative dependencies on system variables are often in quite good agreement. For example, the peak intensity $\hat{S}_{BB}(k^*)$ in the low-temperature regime (which is closely related to T_s) scales with B group fraction as $f_B^{0.69}$ for the nonlinear closure compared with a $f_B^{0.64}$ scaling based on the linear closure.

Predictions of the nonlinear closure have also been obtained for $N_B = 3$ multiblock copolymers with $f_B = 0.9$, 2.4, and 10.4%. Examples of the $\hat{S}_{BB}(k^*)$ peak intensity cooling curves are also shown in Figure 17. Compared to the $N_B = 1$ telechelics, the differences between the linear and nonlinear closure results are qualitatively similar but significantly *smaller* in magnitude. This is because of the enhanced tendency of associating polymers with longer sticky blocks to cluster and the corresponding smaller value of $\beta\epsilon_{BB}$ required. For the nonlinear closure, the lowest temperature numerically attainable corresponds roughly to T_s and values of $\beta\epsilon_{BB} = 4.13$, 3.59, and 2.79 for $f_B = 0.9$, 2.4, and 10.4%, respectively. These are smaller than the corresponding linear closure results by a factor of roughly 3 ($f_B = 0.9\%$) to 1.3 ($f_B = 10.4$). As true for the telechelics, the scaling of the peak intensity $\hat{S}_{BB}(k^*)$ in the low-temperature regime (which is closely related to T_s) with B group fraction are quite similar: $f_B^{0.56}$ for the nonlinear closure compared with a value of $f_B^{0.68}$ based on the linear closure.

In summary, accurate treatment of strong attraction interactions is a difficult theoretical problem within both integral equation theory and all other approaches. For the present work, it is mainly the predictions at very high and very low temperatures that are not qualitatively affected by the linear vs nonlinear closure issue. Interpretation in terms of a reduced temperature, T/T_s, removes most, but not all, of the deviations, as was found previously for diblock copolymers.[19] However, the detailed form of the temperature dependencies for the intermediate regime should be viewed as the least reliable aspect of our work.

Finally, we have investigated briefly the consequences of a using an attractive potential between sticky groups different than the Lennard−Jones (LJ) form of eq 2.1. Calculations for telechelic melts were performed based on a Yukawa potential (which decays more rapidly with separation than the LJ potential) of the form for $r > \sigma$: $V_{BB}(r) = \epsilon_{BB}(\sigma/r)e^{-(r-\sigma)/a}$, for various values of the spatial range parameter "a". When $a = \sigma/4$, the integrated areas under $V_{BB}(r)$ (or equivalently the bare χ_0 of eq 2.2) are nearly the same for both potentials. Smaller values of "a" were also studied to explore the role of a more rapidly spatially varying attraction. For the $a = \sigma/4$ case, comparisons at constant reduced temperature T_s/T led to the following conclusions. (i) In terms of the cooling curve of Figure 4, results based on the Yukawa potential exhibited greater fluctuation stabilization (more nonlinear) and $T_s/T_{ODT} = 1.39$. (ii) Larger absolute values of $\beta\epsilon_{BB}$ at the spinodal (61.1) and ODT (85.0) are found for the Yukawa potential. (iii) $\hat{S}_{BB}(k)$ was slightly less intense, was broader, and peaked at higher wave vector than for the Yukawa model. The differences grow as the range of the Yukawa is reduced. All these differences were rather modest and quantitative in nature. Moreover, they are all consistent with prior PRISM studies of the consequences of spatial range of attractive potentials in diblock copolymer melts and solutions.[19,29,35] Physically, a shorter ranged attractive potential can induce larger structural reorganizations on the local length scales which suppress the growth of microdomain scale fluctuations and lower apparent spinodal and related temperatures.

References and Notes

(1) Eisenberg, A.; Kim, J. S. *Introduction to Ionomers*; J. Wiley & Sons: New York, 1998. Lantman, C. W.; MacKnight, W. J.; Lundberg, R. D. In *Comprehensive Polymer Science*; Allen, G., Bevington, J. C., Eds.; Pergamon Press: Oxford, England, 1989; Vol. 2, Chapter 25.
(2) Sobry, R.; Fontaine, F.; Ledent, J.; Foucart, M.; Jérôme, R. *Macromolecules* **1998**, *31*, 4240.
(3) Williams, C. E.; Russell, T. P.; Jérôme, R. *Macromolecules* **1986**, *19*, 2877.
(4) Venkateshwaran, L. N.; York, G. A.; DePorter, C. D.; McGrath, J. E.; Wilkes, G. L. *Polymer* **1992**, *33*, 2283.
(5) Chu, B.; Wu, D. Q.; Lundberg, R. D.; MacKnight, W. J. *Macromolecules* **1993**, *26*, 994.
(6) Weiss, R. A.; Lefelar, J. A. *Polymer* **1986**, *27*, 3.
(7) Ding, Y. S.; Register, R. A.; Yang, C.; Cooper, S. L. *Polymer* **1989**, *30*, 1213.
(8) Li, C.; Register, R. A.; Cooper, S. L. *Polymer* **1989**, *30*, 1227. Laurer, J. H.; Winey, K. I. *Macromolecules* **1998**, *31*, 9106.
(9) Lee, D.; Register, R. A.; Yang, C.; Cooper, S. L. *Macromolecules* **1988**, *21*, 1005.
(10) Lu, X.; Steckle, W. P.; Hsiao, B.; Weiss, R. A. *Macromolecules* **1995**, *28*, 2831.
(11) Tomita, H.; Register, R. A. *Macromolecules* **1993**, *26*, 2791.
(12) Horrion, J.; Jérôme, R.; Teyssié, Ph.; Marco, C.; Williams, C. E. *Polymer* **1988**, *29*, 1203.
(13) Weiss, R. A.; Fitzgerald, J. J.; Kim, D. *Macromolecules* **1991**, *24*, 1071.
(14) Eisenberg, A. *Macromolecules* **1970**, *3*, 147.
(15) Bates, F. S.; Fredrickson, G. H. *Annu. Rev. Phys. Chem.* **1990**, *41*, 525.
(16) Eisenberg, A.; Hird, B.; Moore, R. B. *Macromolecules* **1990**, *23*, 4098.
(17) Dreyfus, B. *Macromolecules* **1985**, *18*, 284.
(18) Yarusso, D. J.; Cooper, S. L. *Macromolecules* **1983**, *16*, 1871.
(19) David, E. F.; Schweizer, K. S. *J. Chem. Phys.* **1994**, *100*, 7767 and 7784. Guenza, M.; Schweizer, K. S. *J. Chem. Phys.* **1997**, *106*, 7391. David, E. F.; Schweizer, K. S. *Macromolecules* **1997**, *30*, 5180.; Guenza, M.; Schweizer, K. S. *Macromolecules* **1997**, *30*, 4205.
(20) Leibler, L. *Macromolecules* **1980**, *13*, 1602.
(21) Fredrickson, G. H.; Helfand, E. *J. Chem. Phys.* **1987**, *87*, 697.
(22) Matsen, M. W.; Bates, F. S. *Macromolecules* **1996**, *29*, 1091.
(23) Semenov, A. N. *Sov. Phys. JETP* **1985**, *61*, 733.
(24) Lee, D.; Register, R. A.; Yang, C.; Cooper, S. L. *Macromolecules* **1988**, *21*, 998.
(25) Khalatur, P. G..; Khokhlov, A. R.; Kovalenko, J. N.; Mologin, D. A. *J. Chem. Phys.* **1999**, *110*, 6039. Khalatur, P. G.; Khoklov, A. R. *Macromol. Theory Simul.* **1996**, *5*, 877.
(26) Nyrkova, I. A.; Khokhlov, A. R.; Doi, M. *Macromolecules* **1993**, *26*, 3601.
(27) Vilgis, T. A.; Haronska, P. *Macromolecules* **1994**, *27*, 6465.
(28) Bug, A. L. R.; Cates, M. E.; Safran, S. A.; Witten, T. A. *J. Chem. Phys.* **1987**, *87*, 1824.
(29) Schweizer, K. S.; Curro, J. G. *Adv. Chem. Phys.* **1997**, *98*, 1.; *Adv. Polym. Sci.* **1994**, *116*, 319 and references therein.
(30) Chandler, D. In *The Liquid State of Matter*; Montrell, E., Lebowitz, J., Eds.; North Holland: Amsterdam, 1982; p 275.
(31) Chandler, D. *Phys. Rev. E* **1993**, *48*, 2898.
(32) Honnell, K. G.; Curro, J. G.; Schweizer, K. S. *Macromolecules* **1990**, *23*, 3496.
(33) Schweizer, K. S.; David, E. F.; Singh, C.; Curro, J. G.; Rajasekaran, J. J. *Macromolecules* **1995**, *28*, 1528.
(34) Squires, E.; Painter, P.; Howe, S. *Macromolecules* **1987**, *20*, 1740. Register, R. A.; Cooper, S. L.; Thiyagarajan, P.; Chakrapani, S.; Jérôme, R. *Macromolecules* **1990**, *23*, 2978.
(35) Schweizer, K. S.; Yethiraj, A. *J. Chem. Phys.* **1993**, *98*, 9053.
(36) Chatterjee, A. P.; Schweizer, K. S. *J. Chem. Phys.* **1998**, *108*, 3813.
(37) As discussed in the following paper, the failure of numerical convergence seems physically sensible since it seems to often be empirically correlated with formation of B multiplets of roughly maximum space filling density.

(38) Gotze, W.; Sjogren, L. *Rep. Prog. Phys.* **1992**, *55*, 291.
(39) Rosedale, J.; Bates, F. S.; Almdal, K.; Mortensen, K.; Wignall, G. D. *Macromolecules* **1995**, *28*, 1429.
(40) Koberstein, J. T.; Morra, B.; Stein, R. S. *J. Appl. Crystallogr.* **1980**, *13*, 34. The method used to determine interfacial widths is the expanded sigmoidal where $W = (-\text{slope}/4\pi^2 K_p)$ where K_p is the y-axis intercept.
(41) Honnell, K.; McCoy, J.; Curro, J. G.; Schweizer, K. S.; Habenshuss, A.; Narten, A. *J. Chem. Phys.* **1991**, *94*, 4659.
(42) Hansen, J. P.; McDonald, I. R. *Theory of Simple Liquids*; Academic: London, 1991.
(43) Ryan, A. J.; Macosko, C. W.; Bras, W. *Macromolecules* **1992**, *25*, 6277.
(44) Note that we do not include several experimental factors which will broaden the scattering peak such as polydispersity, instrumental smearing, and perhaps background corrections.
(45) Vanhoorne, P.; Van den Bossche, G.; Fontaine, F.; Sobry, R.; Jérôme, R.; Stamm, M. *Macromolecules* **1994**, *27*, 838.
(46) Wang, J.; Li, Y.; Peiffer, D. G.; Chu, B. *Macromolecules* **1993**, *26*, 2633.
(47) Schweizer, K. S.; Fuchs, M.; Szamel, G.; Guenza, M.; Tang, H. *Macromol. Theory Simul.* **1997**, *6*, 1037.
(48) Kolbet, K. A.; Schweizer, K. S. Manuscript in preparation.

MA9912913